RESTRICTED INVESTIGATION REPORT 1525R

CSIRO

INSTITUTE OF ENERGY AND EARTH RESOURCES

Division of Mineral Physics

MAGNETIC PROPERTIES OF ROCKS FROM THE RENISON AREA

D.A. CLARK

P.O. BOX 136,
NORTH RYDE,
NSW AUSTRALIA 2113

MAY 1984

TABLE OF CONTENTS

LIST OF TABLES

LIST OF FIGURES

1. INTRODUCTION

This report presents and discusses results of a collaborative project involving the CSIRO Rock Magnetism Group, Renison Ltd and Mitre Geophysics Ltd. The aims of the project were:

(i) to determine the magnetic properties of Renison-type mineralisation and of other lithologies in the area, in order to provide input to magnetic interpretation and facilitate recognition of the magnetic signatures of Renison-type targets.

(ii) to study the palaeomagnetism of mineralised and unmineralised members of the Crimson Creek Formation with a view to possibly determining or constraining the age of mineralisation and to characterising the thermal history of the area.

(iii) to study the magnetic fabric of ores and country rocks and determine the correlation with local and regional structure.

The sampling programme was carried out in November, 1983 and a preliminary report was submitted to Renison Ltd in February, 1984. A total of 56 samples was collected from the surface and sub-surface.

The lithology and location of the samples are given in Table 1. An attempt was made to sample a variety of mineralisation types from different parts of the mine. Semi-massive to massive ores from the No. 2 and No. 3 dolomite horizons and from the Federal and Melba orebodies are represented. In addition samples of mineralised country rocks (Dalcoath Member, Renison Bell Member and Red Rock Member) adajacent to massive ore zones were collected, as well as unmineralised and weakly mineralised dolomite and unmineralised Red Rock Member. Two samples were also taken from a dolerite dyke in the mine.

On the surface the following rock types were sampled: quartz-feldspar porphyry and adjacent hornfels, Cambrian gabbro, the Crimson Creek Argillite, sediments and spilites of the Dundas Group, and ultramafics of the Serpentine Hill complex.

2. MAGNETIC PETROPHYSICS

The susceptibility (measured along the axis of core samples), NRM intensity and Koenigsberger ratio for the rock samples are listed in Table 2. Because some of the samples are highly anisotropic the bulk susceptibility $\bar{k}$ may differ considerably from the susceptibility k in Table 2. The susceptibility anisotropy and the bulk susceptibility of the samples are discussed in Section 4. The sample NRM directions are given in Table 3.

The quartz-porphyry, spilites and unhornfelsed sediments are very weakly magnetic and should have little expression in magnetic surveys. NRM directions of the sediments and spilite samples are plotted in Fig. 1(a). By contrast the hornfels sample RE01C, which was collected adjacent to the porphyry dyke in the Dalcoath open cut, bears an intense remanence in spite of the relatively low susceptibility. The corresponding Koenigsberger ratio of ~ 50 is typical of baked sediments in the aureole of the Meredith granite, as found by a previous study of the Mt Lindsay prospect. This suggests that quite small porphyry and granite intrusions may be detectable in local magnetic surveys due to the strong magnetic response of their baked contact zones.

The sampled gabbro has relatively low susceptibility but carries quite intense remanence. It can be seen from Table 2 that although the susceptibility values of the four gabbro samples RE02A-D are very consistent the NRM intensities and Koenigsberger ratios are very variable. This inhomogeneity is emphasised by the disparity in the NRM directions in Table 3. The NRM of the more intensely magnetised samples (2A and 2C) is of normal polarity and is consistent with the remanence direction with steep negative inclination which is characteristic of most of the rock types represented in this study.

Samples RE02B and RE02D, on the other hand, have significantly lower Q values (7 and 16 as against 32 and 58) and have reversed remanence, directed SSW with shallow positive inclination. Because 2B and 2D were drilled from a different, but adjacent, outcrop to 2A and 2C the difference in NRM directions could be explained if one or both of the

large blocks from which the samples were drilled was not in situ. However the correlation of NRM direction with other magnetic properties (J and Q) suggests that the disparity arises from multicomponent remanence. Furthermore, the consistency of the magnetic fabric exhibited by the four gabbro samples, which will be discussed in Section 4, implies that all samples are almost certainly correctly oriented.

Palaeomagnetic cleaning of the gabbro samples demonstrates that the remanence of the two groups of samples is different in character - the NRM of the normally magnetised samples appearing to be single component, whereas there is evidence of at least two remanence components in samples 2B and 2D. However the various magnetisation components could not be fully resolved and an unambiguous evaluation of representative remanence intensities and directions for the gabbroic pluton would require further sampling.

The results of palaeomagnetic cleaning of the gabbro samples indicate that the measured NRMs are probably intrinsic to the lithology and are not simply a reflection of surface effects such as weathering or lightning strikes. On this basis plausible estimates of the average remanence and Koenigsberger ratio are J $\simeq$ 2,000 microgauss (200 gammas) with dec $\simeq 240°$, inc $\simeq -50°$, and Q $\simeq$ 20. If these values are at all representative a substantial magnetic anomaly should be associated with this pluton.

The ultramafics, with the exception of the weathered sample from site 4, are strongly but variably magnetic. The NRM directions of the fresh ultramafic samples are rather scattered, as can be seen from Fig. 1(b). However all the directions lie on the upper hemisphere and are predominantly N-NE with moderate to steep negative inclinations.

The mean susceptibility for the thirteen fresh ultramafic samples is, from Table 2, 4300 x 10^{-6} with standard error 1000 x 10^{-6}. The mean Koenigsberger ratio is 3 $\pm$ 1 indicating that remanence is the dominant contributor to magnetic anomalies associated with the ultramafics. The effective Q value within any unit will be reduced by scatter of the NRM directions but remanence should make a substantial contribution to the nett magnetisation of the ultramafics.

There is a considerable sampling problem with the ultramafic rocks because of the small-scale inhomogeneity associated with irregular distribution of magnetite. Most of the magnetite is confined to the joint planes in these highly fractured rocks. An added complication is the pronounced susceptibility anisotropy arising from self-demagnetisation normal to the plane of highly magnetic layers.

The magnetic mineralogy of a sample of serpentinised ultramafic (RE09D) was investigated using thermomagnetic analysis. The variation of susceptibility with temperature is shown in Fig. 3(a). The form of the heating curve indicates the presence of an unstable phase, probably maghaemite, which contributes ~ 20% to the room temperature susceptibility of the rock. This phase breaks down above ~ 450°C, as indicated by the irreversibility of the k-T curve on subsequent cooling from 650°C. The dominant magnetic mineral initially in the rock and the only magnetic phase present after the heating is almost pure, predominantly multidomain, magnetite with a Curie temperature of 600°C.

The NRM directions of the mineralised samples RE10A-E, RE11A-C, R12A-C, RE14E and RE15A-D are plotted in Fig. 2. Although there is considerable scatter, directions with steep negative inclinations predominate. Samples taken from the No. 2 dolomite, Federal 2000, Melba 2015 and the Red Rock Member adjacent to No. 2 ore have fairly well-grouped directions, whereas NRM directions of No. 3 ore samples are scattered.

Low field thermomagnetic (k-T) curves of selected ore samples are shown in Figs. 3-5. Reversible curves with a single Curie temperature at ~ 330°C indicate monoclinic pyrrhotite (e.g. RE14E in Fig. 5(a)). Monoclinic pyrrhotite has 4C superstructure and composition ~Fe_7S_8.

Thermomagnetic curves showing considerable thermal hysteresis with prominent peaks in susceptibility at ~ 250°C indicate the presence of hexagonal (intermediate) pyrrhotite with composition ~Fe_9S_{10}, as well as monoclinic pyrrhotite. Most samples contain hexagonal and monoclinic pyrrhotite. Massive pyrrhotite from the Mt Lindsay prospect, by contrast, consists entirely of hexagonal pyrrhotite, as was shown in a previous study.

Samples RE12A and RE15B (Figs. 4(b) and 5(b)) typify the behaviour of samples rich in hexagonal pyrrhotite. At room temperature only monoclinic pyrrhotite contributes substantially to the susceptibility because hexagonal pyrrhotite is antiferromagnetic at low temperatures and has very low susceptibility. At about 200°C vacancy re-ordering commences in the hexagonal pyrrhotite and a ferrimagnetic superstructure is formed leading to a sharp increase in susceptibility. Because the vacancy diffusion is relatively slow below 300°C the curve is more or less irreversible in the region of the susceptibility peak - if the sample is quenched from ~ 250°C the peak susceptibility is preserved, whereas very slow cooling will essentially retrace the initial heating curve. At ~ 300°C the vacancies disorder, the ferrimagnetic structure breaks down and the susceptibility of the hexagonal pyrrhotite essentially vanishes leaving only the contribution of the monoclinic pyrrhotite. Above ~ 310° the susceptibility of the monoclic pyrrhotite drops rapidly to a very low value at the Curie temperature. On subsequent cooling of the pyrrhotite mixture (which by this stage is usually partly homogenised) the susceptibility increases sharply at the Curie temperature and then further at the vacancy-ordering temperature. The ferrimagnetic structure of the hexagonal pyrrhotite cannot re-equilibrate to the antiferromagnetic structure which is stable below 200°C, producing the grossly irreversible curves shown.

The magnetic mineralogy of the ore samples subjected to thermomagnetic analysis can be summarised as:

(i) Monoclinic pyrrhotite only - RE13B, RE14E
(ii) Monoclinic + hexagonal - RE10D, RE11B
(iii) Hexagonal + monoclinic - RE12A, RE15B

Patterson (1979) states that monoclinic pyrrhotite commonly occurs as lenticular or flame-like bodies within a host of hexagonal pyrrhotite, and occasionally vice versa.

The susceptibility of Renison massive pyrrhotite will therefore be reduced with respect to massive coarse-grained monoclinic pyrrhotite due both to dilution by the non-magnetic hexagonal phase and to reduction of

the effective grain-size of the monoclinic pyrrhotite. The most important parameter is the volume fraction of monoclinic pyrrhotite. Assuming an effective grain-size of ~ 100 μm the corresponding emu susceptibility of monoclinic pyrrhotite grains is about 0.03. If the pyrrhotite fraction of the ore is f_{Po} and the fraction of the total pyrrhotite content which is monoclinic is f_{MPo}, then the susceptibility of the ore is ~ 0.03 f_{Po} f_{MPo}. For example, if 30% of the pyrrhotite is monoclinic and the total pyrrhotite content is 90%, k ≃ 0.008. Using this approach the overall susceptibility of the orebodies can be roughly estimated from a knowledge of typical pyrrhotite contents. The contribution of remanent magnetisation can then be estimated from the Koenigsberger ratios and NRM directions of ore samples.

The average susceptibility of the 14 samples collected from massive ore zones is 7,000 x 10^{-6} with standard deviation 4,700 x 10^{-6}. This mean value corresponds to a monoclinic pyrrhotite content of ~ 25% of the total ore. The data of Haynes and Hill (1970) give a mean value of 56% for f_{MPo} for 33 massive ore samples from DDH 48 and DDH 60. Hutchinson (1979) found f_{Po} ≃ 85% and f_{MPo} ≃ 20% for five samples from the Colebrook orebody. The mean Koenigsberger ratio of the same samples is 2.5 (s.d. 2.2) and this value is not significantly changed if the Q values of the weakly mineralised samples are added in. In view of the systematic grouping of NRM directions, remanence contributes substantially to the overall magnetisation. The effective remanent magnetisation is in the same general sense as the induced magnetisation and about twice as strong.

3. PALAEOMAGNETISM

Palaeomagnetic cleaning enables resolution of remanence components acquired at different times which, in favourable circumstances, may be related to the age of formation of the rock and subsequent geological events. Samples may also acquire various sorts of palaeomagnetic noise which are unrepresentative of the bulk of the rock unit. Cleaning can often remove these spurious remanence components, thus enhancing the utility of magnetic property measurements. AF cleaning is particularly efficacious in removing isothermal remanent magnetisations (remanence components acquired at ambient temperatures due to exposure to high magnetic fields) whereas thermal demagnetistion readily removes viscous remanence acquired during prolonged exposure to a weak magnetic field.

The palaeomagnetic cleaning of each rock type will be discussed in turn. The results are presented in the form of vector diagrams. These plots depict the end-points of remanence vectors measured after each demagnetisation step, projected onto orthogonal planes. The horizontal plane is always taken as one of the projection planes, the other is either the N-S or E-W vertical plane. For conciseness the two projections are usually combined into a single diagram with small circles representing vector end-points projected onto the vertical plane and crosses representing horizontal components. Linear segments of the plots (i.e. sets of consecutive demagnetisation steps for which both the corresponding circles and crosses define straight lines) indicate consistent removal of a single remanence component (i.e. a remanence vector of constant direction). Curved segments indicate two or more components of magnetisation with overlapped stability spectra over the corresponding range of demagnetisation steps. Commonly, distinct remanence components, acquired at different times, have partially overlapped stability spectra. In this case the vector plots consist of a series of linear segments, corresponding to resolved components, joined by curved sections, which correspond to unresolved, hybrid components. The most stable component is resolved if the final linear segment is directed towards the origin of the plot.

Gabbro

Thermal demagnetisation data for specimens from each of the four gabbro samples are depicted in Fig. 6. The corresponding plots for AF cleaning are similar. Figs. 6(a) and 6(c) show that the directions of the normally magnetised samples RE02A,C hardly change on thermal cleaning. A well-defined component is consistently removed above 200°C until the remanence is totally destroyed at 350°C.

By contrast, the NRM of the reversely magnetised samples is a multicomponent remanence, although the various components present could not be fully resolved.

The thermal stability of the remanence borne by the normally and reversely magnetised samples appears to be somewhat different, as a

residual component in the reversely magnetised rocks survives above 350°C. This possibly indicates a chemical difference between the remanence carriers in the two types of sample. The remanence components in both the normally and reversely magnetised samples appear to be ancient magnetisations, acquired at widely different times in the two types. With the limited number of samples no definite conclusions about the age and nature of the remanence components can be drawn.

Sediments and Spilites

The sediments and spilites are very weakly magnetised and in many cases only limited demagnetisation could be carried out before the residual remanence dropped below the noise level of the measuring instruments. However AF and thermal cleaning of the more strongly magnetised samples indicates that the NRMs are essentially single-component. The high thermal stability of the NRM directions demonstrates that the ubiquitous steeply upward-pointing component is not simply a viscous remanence acquired recently.

The stability and consistency of NRM directions in these rocks over a wide area suggests that the NRMs reflect a pervasive thermal event, which should also have affected the orebodies. The implications of the results from the country rocks for the magnetisation of Renison-type mineralisation will be considered in the discussion at the end of this section.

Ultramafics

Representative vector diagrams for thermal and AF demagnetisation of specimens of the ultramafic samples are shown in Fig. 7. The response to AF and thermal cleaning for these samples is similar. The curves shown in 7(a) and 7(c) indicate the presence of several (probably three) apparently sub-parallel components, with overlapped stability spectra. The most stable component is generally northwards with shallow negative inclination and is clearly ancient.

Overlapped thermal stability spectra are diagnostic of remanent magnetisation associated with grain growth or chemical change in the magnetic grains (chemical remanent magnetisation). As a result of this process the less stable remanence components are not well-resolved and are therefore difficult to interpret.

Another complication is the relatively high susceptibility anisotropy of the ultramafics, ranging from 1.1 to 1.9, which tends to deflect remanence directions towards the plane of high susceptibility. AF cleaning tends to counteract this bias. This may account for the better resolution of the remanence components by AF demagnetisation, which is evident in several cases from comparison of AF and thermal demagnetisation results for specimens from the same sample. Examples of clearly resolved components are shown in Figs. 7(b) and 7(d).

The simplest interpretation of the data is that the characteristic component, northward with shallow negative inclination, represents an overprint magnetisation associated with thermal metamorphism during the episode of extensive granite intrusion in the Renison Bell area.

Sulphide Ores

The responses of selected specimens from sulphide ore samples to palaeomagnetic cleaning are depicted in Figs. 8-13. The ore samples fall into two categories: No. 2 dolomite horizon, Federal and Melba ores, which have relatively simple magnetisations; and No. 3 dolomite horizon ores (sites 11 and 15) which exhibit complex behaviour.

Overall the behaviour is quite variable - the linear segments in vector plots are noisy on some cases (e.g. Fig. 8(a)) and well-defined in other cases (e.g. Fig. 8(b)), the NRMs are multicomponent in some specimens (e.g. Fig. 9(a)) and essentially single-component in other specimens (e.g. Fig. 10(c)). In many cases the most stable component is resolved, but in some specimens the final linear segment is clearly missing the origin (see e.g. Fig. 9(d)), implying that there is a residual component which has not been isolated by the cleaning.

Directions with steep negative inclinations predominate for components of low, intermediate and high stability, accounting for the sub-vertical NRM directions which characterise the ore samples.

In Fig. 11(c)-(d) vector plots for specimens from a thin dolerite dyke cutting No. 2 ore at Site 14 are shown for comparison with ore samples. The characteristic component isolated by AF and by thermal cleaning is NW with very steep negative inclination. Because of its high stability this component is probably primary. A palaeomagnetic pole cannot be calculated for the dolerite because only two samples were collected and because rapid cooling of the dyke would give a spot reading of the geomagnetic field rather than a time-averaged field corresponding to an axial geocentric dipole. However the observed remanence direction is consistent with a Jurassic age, suggesting that the dyke may be coaeval with the Tasmanian dolerite sills - in accordance with the chemical and petrologic similarity of the dyke to the sills.

The demagnetisation trend of specimen RE14E2 is straightforward (see Fig. 11(a)) but the behaviour of a sister specimen RE14E4 is more complex with two components present (Fig. 11(b)). The more stable component, SE with positive inclination, may be a self-reversed equivalent of the predominant components with negative inclination, as partial self-reversal is known to occur in some pyrrhotite-bearing rocks.

The behaviour of specimen RE14E4 is reminiscent of the complicated demagnetisation trends of samples from sites 11 and 15, which are illustrated in Figs. 12 and 13. In most cases a steeply upward-pointing component of low to intermediate stability is present, but stable components are either not resolved (e.g. Figs. 13(c)-(d)), are noisy and inconsistent from sample to sample (e.g. Figs. 12(b)-(c)) or show complex behaviour suggestive of partial self-reversal or interaction between different magnetic phases (e.g. Figs. 12(a) and 12(c)). This complexity may arise from magnetic interaction between intergrown monoclinic and hexagonal pyrrhotites. The palaeomagnetic data from the No. 3 dolomite horizon ores are therefore difficult to interpret.

Discussion

The various remanence components isolated by palaeomagnetic cleaning appear to be secondary magnetisations related to thermal events. Because magnetisations corresponding to distinct overprinting episodes may have overlapped coercivity spectra and therefore may not be well resolved by AF cleaning, only results from thermal demagnetisation were used for quantitative interpretation. The AF cleaning data serve, however, as qualitative confirmation of the conclusions derived from thermal cleaning.

The most thermally stable components from all specimens of a particular rock type for which these components were well-resolved were combined to calculate a formation mean direction and palaeomagnetic pole. The age of magnetisation could then be estimated by comparison of the calculated pole with the Phanerozoic Australian apparent polar wander path (Embleton, 1981; Goleby, 1980). The individual well-resolved high temperature components, formation mean directions and 95% cones of confidence for the sediments and spilites, ultramafics and ores (mineralised No. 2 dolomite, Melba and Federal) are plotted in Figs. 14, 15 and 16 respectively.

The calculated formation mean directions and corresponding palaeomagnetic poles are listed in Table 4. Some specimen directions which are clearly outliers are indicated in Figs. 14-16 and are excluded from the calculation of the mean directions.

The high temperature ($\sim$ 350-550°C) magnetisation carried by the sedimentary and spilitic country rocks is close to the present field direction but is clearly distinct from the dipole field direction, as can be seen from Fig. 14. If this component were of viscous origin it could only have been acquired over a very short time span ($<$ 1000 years) in order to have completely failed to average secular variation (and thus only reflect the anomalously steep field of the very recent past at this locality). Such a component would be completely destroyed by thermal demagnetisation to 200°C, or less.

Hence this component appears to be a stable ancient magnetisation. The preferred interpretation is that the high temperature magnetisation of

these rocks reflects a pervasive thermal overprint, probably in the Jurassic. This thermal overprint may be related to the major episode of dolerite sill injection which took place in Tasmania during the mid-Jurassic (170 m.y.).

The high temperature magnetisation carried by the ultramafics appears to be considerably more ancient than this, because of its shallow inclination. The geomagnetic field in South-eastern Australia has been consistently steep since the Carboniferous. The probable age of this magnetisation is late Devonian and it is inferred to arise from thermal metamorphism associated with granite intrusion. Low and intermediate temperature components of magnetisation carried by the ultramafics are rather scattered but are generally steeper, i.e. biased towards the present field or the Jurassic overprint direction.

The remanence of the country rocks is predominantly carried by magnetite, which has a Curie temperature of 580°C, whereas the remanence of the mineralised samples is carried by monoclinic pyrrhotite, which has a Curie temperature of 330°C and is therefore more easily reset by thermal events.

The "high temperature" components from the well-behaved mineralised samples are generally defined over a temperature range whose lower limit is ~200-270°C and whose upper limit is ~300-330°C. From Fig. 16, the mean direction is clearly distinct from present field and dipole field directions and is therefore ancient. The most probable age of magnetisation is mid-late Jurassic (c. 140 m.y.), suggesting that the magnetisation was blocked in during slow cooling following the major thermal event in the mid-Jurassic.

The palaeomagnetic data from the Renison area can be interpreted as follows:

(i) the pre-Devonian rocks were extensively remagnetised by thermal metamorphism in the late Devonian.

(ii) a pervasive, relatively low grade event in the Jurassic partially remagnetised the ultramafic rocks with magnetic carriers of high

thermal stability and fully remagnetised the sedimentary and spilitic rocks, containing fine-grained magnetite and/or haematite of moderate thermal stability, and the pyrrhotite-bearing rocks of relatively low thermal stability.

Using theoretical time-temperture-magnetisation relationships given by Middleton and Schmidt (1982) for magnetite and haematite and by Clark (1983a) for pyrrhotite, the suggested maximum temperature of this event is ~200°C. It is possible that the sediments and spilites may retain small, thermally stable, pre-Jurassic remanence components, but these could be difficult to detect with the present equipment due to the weak magnetisation of these rocks.

(iii) The thermal event peaked in the mid-Jurassic and was followed by a prolonged period of cooling. The magnetisation of the sediments and spilites was blocked in soon after the peak of the mid-Jurassic thermal event, whereas the magnetisation carried by pyrrhotite was blocked in ~ 30 m.y. later.

In order to account for the postulated temperatures attained during the Jurassic it is necessary to postulate the presence of Upper Carboniferous-Triassic sediments of the Parmeener Super Group overlying the Renison area, which were extensively intruded by dolerite sills in the mid-Jurassic. These postulated sediments and sills have since been eroded, possibly following opening of the Southern ocean, but remnant patches are exposed approximately 20 km W, 25 km SW, 12 km SSE, 32 km SE, 28 km NE and 50 km NNW of Renison Bell. Because of the very high equivalent goethermal gradient which would have been associated with the sill injection, the thickness of the sediments need not have been very great - possibly as little as 1-2 km.

The effect of this thermal event on the mineralogy of the rocks of the Renison area would probably be undetectable, both because of the relatively low temperatures and pressures involved and because of the earlier regional metamorphism and pervasive thermal metamorphism associated with Devonian granites.

The following arguments lend support to the hypothesised Jurassic event:

(i) major dolerite sills intruding Parmeener Super Group sediments are ubiquitous in central and Eastern Tasmania. In addition, there are extensive exposures North of Savage River and between Wynyard and Mt Bischoff, and numerous outliers in western Tasmania,

(ii) the Tasmanian dolerites are correlated with extensive Jurassic intrusions in contiguous Gondwanaland continents - the Ferrar dolerites in Antarctica and the Karroo dolerites in southern Africa - indicating that intrusion of the Tasmanian dolerites was part of a major geological event and suggesting that the distribution of dolerite sills in Tasmania could formerly have been far more extensive. In Antarctica, pervasive thermal metamorphism is associated with the Ferrar dolerites,

(iii) the mine area is intruded by a dolerite dyke, probably coaeval with the Jurassic sills. Although the contact metamorphic effects of this thin dyke are minimal, its presence indicates the occurrence of basaltic magmatism in the area during the Jurassic.

These arguments for the proposed model are indirect and by themselves are not conclusive. Direct confirmation of the occurrence of a major thermal event in the mid-Jurassic, followed by low cooling, would probably rely on fission track dating of zircon, sphene and apatite from western Tasmanian rocks or of Ar40-Ar39 dating of suitable rock types from the area. The hypothesis should also be tested against any relevant geological and geomorphological evidence.

4. MAGNETIC FABRIC

Most of the sampled rock types have a measurable susceptibility anisotropy and the ultramafics and sulphide ores are highly anisotropic. Because the susceptibility ellipsoids of individual specimens of each rock type tend to be systematically oriented, they define a magnetic fabric which can be interpreted in terms of microfabric and mesoscopic structures.

The magnetic lineation is parallel to the major (k_1) susceptibility axis and the magnetic foliation plane contains the major and intermediate (k_2) susceptibility axes. The pole to the magnetic foliation is therefore parallel to the minor (k_3) susceptibility axis. The anisotropy magnitude A is defined as k_1/k_3 and the bulk susceptibility $\bar{k} = (k_1 + k_2 + k_3)/3$. The bulk susceptibility is a useful quantity because it is equal to the mean susceptibility measured along any three mutually perpendicular directions.

The strength of the magnetic lineation is given by $L = k_1/k_2$ and the magnetic foliation strength is $F = k_2/k_3$. The prolateness P is given by L/F and is a useful parameter for characterising deformational fabrics. $P > 1$ implies that lineation is the dominant feature of the fabric and is generally correlated with an elongated strain ellipsoid. $P < 1$ implies that foliation is dominant and is associated with strain in the field of flattening. Summaries of the concepts, physical principles and applications of magnetic fabric studies are given by Clark and Embleton (1980) and Clark (1983b).

The parameters $\bar{k}$, A, L, F, P are listed in Table 5. Because of the high frequency of operation (10 kHz) of the Digico anisotropy delineator on which the susceptibility anisotropy was measured, the results from highly conductive sulphide samples may be affected by induced eddy currents. For this reason the results from the Digico were tested against measurements on a low frequency (211 Hz) susceptibility bridge. For all cases except samples 15B-D the results were acceptable.

For the ultramafic specimens the measured susceptibility axis magnitudes may be unrepresentative of the rock formation because the magnetic fabric is due primary to textural anisotropy on a mesoscopic to macroscopic scale which is comparable to, or larger than, the size of the samples. However there is probably a close correspondence between the susceptibility axis directions of the samples and the formation as a whole.

The directions of the well-defined sample mean magnetic lineations and foliation poles are given in Table 6. Major and minor susceptibility

axis directions for specimens or samples from particular rock types or sites are shown in Figs. 17-20.

Gabbro

The gabbro from site 2 exhibits a well-defined magnetic lineation plunging steeply to the south (see Fig. 17(a)). The foliation poles are scattered, apparently randomly, around the girdle orthogonal to the lineation. This is consistent with the linear parallel nature of the fabric, indicated by the prolate susceptibility ellipsoids ($P > 1$). The magnetic fabric may reflect the mode of emplacement of the gabbro pluton - the magnetic lineation indicating the direction of magma flow. The present off-vertical orientation of the lineation could result from tilting of the body through ~25°C, or it may reflect emplacement from a source lying to the south. However deformational origin is also possible.

Crimson Creek and Dundas Sediments and Spilites

The sample from the Crimson Creek Formation in the vicinity of Pine Hill has a magnetic foliation dipping ~45°C to the east, which contains a lineation plunging E at ~45°C (Fig. 17(b)). The magnetic foliation is probably parallel to bedding and is consistent with the probable closure of the Renison Bell anticline in the vicinity of Commonwealth Hill. The magnetic lineation may reflect extension parallel to the axes of eastward plunging subsidiary folds.

The magnetic foliation of the Dundas Group samples from site 5 is not as well developed, but there is a suggestion from Fig. 17(c) that the foliation dips steeply to the east. The mean magnetic lineation is quite well-defined, plunging very steeply to the SSE.

The magnetic fabric of the spilites (Figs. 17(c) and 18(b)) shows eastward-dipping foliations, but the dip is variable and the lineations are quite different at the two sites - at site 6 the linetion is N-S horizontal and at site 8 it plunges steeply to the SE.

Ultramafics

The ultramafics from site 7 (Fig. 18(a)) have well-grouped susceptibility axis directions with a foliation striking ENE and dipping steeply SSE containing a down-dip lineation. The magnetic fabric of the serpentinised ultramafics at site 9 is very confused, but the three block samples 9H-J gave consistent results - defining a sub-vertical WNW-striking foliation with a lineation plunging shallowly to the ESE (Fig. 18(c)). At both these sites the effective susceptibility would be enhanced by the favourable orientation of the plane of high susceptibility. The magnetic foliation in the ultramafics reflects the pattern of jointing and probably tends to parallel the faulted margins of the ultramafic complex.

No. 2 Dolomite

The unmineralised and weakly mineralised samples of the No. 2 dolomite have a consistent N-S magnetic foliation dipping steeply to the west (Fig. 18(d)). This contrasts with the subhorizontal foliation of the semi-massive to massive stratabound ores and to the easterly-dipping foliations of the magnetite-bearing rocks in the mine (Red Rock Member) and on the surface.

Stratabound ores

The pyrrhotite-rich stratabound ores from sites 10, 11 and 15 have consistently steep foliation poles, indicating a sub-horizontal magnetic foliation. Where a magnetic lineation is well-defined it is either N-S or E-W horizontal, indicating that major and intermediate susceptibility axes interchange from place to place in the stratabound ores. This bimodal distribution of horizontal magnetic lineations also agrees with lineations from some country rock and weakly mineralised samples from sites 3, 6, 10 and 16.

The effective susceptibility of the stratabound ores in the steep ambient field is reduced by the sub-horizontal orientation of the plane of high susceptibility. Assuming an isotopic foliation plane (L = 1) and

taking A ≃ 2, we find that the induced magnetisation is deflected ~ 15° towards the horizontal and is reduced by ~30% from the value kF. This emphasises the dominance of remanence in the magnetisation of these ores.

Federal ore

The magnetic foliation at site 12 strikes NW and dips steeply to the NE, parallel to the Federal-Bassett fault (Fig. 20(a)). This fabric evidently results from shear deformation associated with faulting. The magnetic lineation plunges ~35° to the SE.

Melba ore

Although the Melba ore is highly disrupted, the magnetic fabric is similar to the stratabound ores (Fig. 20(b)) indicating that the magnetic fabric is post-brecciation. The foliation is sub-horizontal with a N-S lineation.

Dolerite

The two samples from the dolerite dyke at site 14 exhibit a well-defined NW-striking vertical magnetic foliation containing a sub-vertical lineation, plunging very steeply SE (Fig. 20(c)). The foliation plane is interpreted as the plane of the dyke with the lineation representing the flow direction.

Red Rock Member

The samples of Red Rock Member collected from sites 14 and 16 exhibit a mean magnetic foliation dipping shallowly NE. This is regarded as a bedding parallel foliation.

Discussion

The magnetic fabric of the weakly magnetic country rocks reflects the preferred dimensional orientation of the small fraction of magnetite grains contained within them. The most plausible interpretation of the magnetic fabric of these low grade, weakly deformed metasediments and

metavolcanics is that the foliation is bedding-parallel and the lineation usually indicates the direction of maximum extension.

The sampling of these rocks was very sparse and is inadequate to characterise the deformation in the area, particularly in view of the known complexity of folding. However a predominance of E-SE dips in the vicinity of Pine Hill and the NE Dundas tramway is suggested. The distribution of bedding poles also suggests a N-NE axis of folding, corresponding to the subsidiary folds in the mine area described by Patterson (1979).

The magnetic lineations tend to have moderate to steep SE plunge. This is similar to the lineations in the Mt Lindsay area, suggesting that this fabric element is of regional extent and reflects a common direction of extension determined by a regional stress field.

The magnetic lineation of the gabbro is also due to alignment of long axes of magnetic grains and may be related to the emplacement of the pluton. However the coincidence of the lineation direction with the regional magnetic lineation in the country rocks suggests that the lineation in this case may also be deformational.

By contrast, the magnetic fabric of the ultramafics is predominantly textural, arising from the self-demagnetisation of magnetite-rich layers within the rock. Magnetite is preferentially developed in fractures, producing a magnetic foliation parallel to the dominant joint plane. At sites 7 and 9 the trend of the magnetic foliation appears to parallel the nearest faulted margin of the ultramafic complex.

Magnetic fabric of pyrrhotite-bearing rocks arises in a different way to that of magnetite-bearing rocks. Pyrhotite crystals have strong intrinsic magnetic anisotropy and preferred crystallographic orientation of pyrrhotite grains produces a pronounced magnetic fabric. The minor susceptibility axis corresponds to the preferred alignment of crystallographic c-axes, the magnetic foliation therefore coinciding with the preferred basal plane orientation.

In pyrrhotite ores, there is generally a close correlation between crystallographic alignment and preferred dimensional orientation of pyrrhotite grains (Clark, 1983b). This reflects the highly ductile nature of pyrrhotite, which responds readily to applied stress, especially, at elevated temperatures (>100°). Ductile flow takes place mainly by gliding on slip planes parallel to the basal plane and results in a coincidence of basal plane preferred orientation (hence magnetic foliation) and conventional foliation.

Renison pyrrhotite exhibits distinct preferred orientation and is extensively recrystallised (Hutchinson, 1979; Patterson, 1979). Textural evidence of deformation is abundant in pyrrhotite grains.

The susceptibility anisotropy of the ores not only confirms the high degree of preferred orientation of pyrrhotite but defines the attitude of the fabric, which may not always be apparent from petrographic studies on unoriented samples.

The magnetic foliation of the stratabound ores and Melba ore is horizontal, slightly discordant to bedding, and is therefore not mimetic of the primary bedding-parallel fabric of the host rocks. This confirms the deformational origin of the pyrrhotite fabric. Furthermore, the fabric must post-date the brecciation of the mineralised Renison Bell Member (Melba ore).

The magnetic fabric of these ores is interpreted to represent ductile flow and/or recrystallisation of pyrrhotite-rich layers and regions in response to a stress field with a vertical axis of maximum compression, probably at temperatures below 300°C (based on textural evidence).

The other principal axes of the stress field were N-S and E-W, but their identification as axes of intermediate and least compressive stress is ambiguous. This stress field, and the acquisition of the associated fabric, may correspond to the Jurassic thermal event inferred from the palaeomagnetism.

The stress field within the Federal-Bassett fault zone was evidently quite different, as seems intuitively plausible. The magnetic foliation at site 12 represents the response to shear deformation accompanying fault movement. The magnetic fabric of all ore types is predominantly planar parallel, as indicated by the oblate ($P<1$) ellipsoids.

The isolated pyrrhotite grains within the weakly mineralised No.2 dolomite samples appear to have been protected by the rock matrix and retain an earlier, steeply westward-dipping foliation. This may represent an incipient cleavage, possibly axial planar to N-S trending folds.

5. CONCLUSIONS

1. Quartz-feldspar porphyry, unhornfelsed sediments and spilites were found to be very weakly magnetic. Fresh ultramafics, and massive pyrrhotite are strongly magnetic and should be associated with prominent magnetic anomalies. Gabbro samples were found to be moderately magnetic. A hornfels sample carried intense remanence suggesting that buried granitic intrusives may be detectable by the magnetic signatures of their metamorphic aureoles.

2. The characteristic NRM direction of the ultramafic rocks is northward with moderate negative inclination. NRMs of ore samples, sediments and spilites are predominantly directed steeply upwards. The relative consistency of NRM directions and the high Koenigsberger ratios of the strongly magnetic samples indicate that remanence is important to interpretation, the main effect being to enhance greatly the effective susceptibility as the remanence is generally sub-parallel to the induced magnetisation.

3. Semi-quantitative analysis of monoclinic pyrrhotite, hexagonal pyrrhotite and magnetic contents of ore samples can be rapidly carried out by means of thermomagnetic curves. This technique could be readily used to characterise the distribution of pyrrhotite types within a deposit.

4. Palaeomagnetic cleaning and statistical analysis of remanence components demonstrate that the NRMs of the samples from the Renison area are dominated by secondary, but ancient, components which can be attributed to thermal overprinting. The inferred magnetic history encompasses:

(i) remagnetisation, probably associated with granite emplacement in the Late Devonian, producing a component with mean direction dec = 20°, inc = -21° which is preserved by magnetite grains with higher blocking temperatures in the ultramafics,

(ii) overprinting or reprinting, depending on maximum blocking temperatures, of the earlier magnetisation by a pervasive but relatively low grade thermal event, peaking at ~200°C in the mid-Jurassic, followed by slow cooling. This thermal event is inferred to be associated with the major Jurassic dolerite sill emplacement in Tasmania, Antarctica and Africa, which preceded the breakup of Gondwanaland. The most thermally stable remanence component was blocked at ~170 m.y. in the magnetite-bearing country rocks (sediments and spilites) and somewhat later, about 140 my, in the pyrrhotite-bearing rocks. The destruction of primary remanence by a subsequent thermal event precludes determination of an age of mineralisation on the basis of palaeomagnetic data.

5. The above explanation for the palaeomagnetic data implies that the remanence of rocks in western Tasmania will generally reflect Jurassic overprinting and directions with steep negative inclinations should predominate.

6. The magnetic foliation of the country rocks appears to be bedding-parallel. The distribution of foliation poles indicates some structural complexity with more than one generation of folding. In the area of Pine Hill and the NE Dundas tramway SE-dipping foliations predominate and a N-NE axis of folding is suggested by the data.

7. The magnetic foliation of the Federal ore dips steeply to the NE,

parallel to the Federal-Bassett fault, and probably reflects shearing in the fault zone. The magnetic foliation of the stratabound and Melba ores is flat-lying and is interpreted to result from ductile flow and/or recrystallisation of the pyrrhotite in a stress field with a vertical axis of maximum compression. This deformational pyrrhotite fabric may date from the Jurassic thermal event inferred from the palaeomagnetism. Disseminated pyrrhotite in the No.2 carbonate preserves a, presumably earlier, magnetic foliation dipping very steeply west, possibly representing an incipient cleavage.

6. REFERENCES

Clark, D.A. and Embleton, B.J.J., 1980. Applications of Rock Magnetism to Mineral Exploration. CSIRO Restricted Investigation Report 1193R.

Clark, C.A., 1983a. Palaeomagnetism of Pyrrhotite-bearing Rocks. CSIRO Restricted Investigation Report 1438R.

Clark, C.A. 1983b. Magnetic Fabric of Pyrrhotite-bearing Rocks. CSIRO Restricted Investigation Report 1462R.

Embleton, B.J.J., 1981. A review of the paleomagnetism of Australia and Antarctica. In: M.W. McElhinny and D.A. Valencio (editors), Paleoreconstruction of the Continents. American Geophysical Union, Geodynamics Series, volume 2.

Goleby, B.R., 1980. Early Palaeozoic palaeomagnetism in south east Australia. J. Geomag. Geoelectr., 32, Suppl. III: 11-21.

Haynes, S.J. and Hill, P.A., 1970. Pyrrhotite phases and pyrrhotite-pyrite relationships, Renison Bell, Tasmania. Econ. Geol., 65: 838-848.

Hutchinson, R.W., 1979. Evidence of exhalative origin for Tasmanian tin deposits. CIM Bull., 72: 90-104.

Middleton, M.F. and Schmidt, P.W., 1982. Paleothermometry of the Sydney Basin. J. Geophys. Res., 87: 5351-5359.

Patterson, D.J., 1979. Geology and Mineralization at Renison Bell, Western Tasmania. Ph.D. thesis, University of Tasmania.

TABLE 1. LITHOLOGY AND LOCATION OF SAMPLES

Sample	Rock type	Locality
RE01A-B	Quartz porphyry	Dalcoath open cut
RE01C	Hornfels	" " "
RE02A-D	Gabbro	
RE03A	Crimson Creek Formation	Open cut on Pine Hill Road
RE04A	Weathered Ultramafic	30m N of 3400N peg
RE05A-B	Dundas sediment	NE Dundas tramway
RE06A-B	Spilite	Dundas tramway 300m S of air photo marker
RE07A-C	Ultramafic	Side track from tramway
RE08A-D	Spilite	Dundas tramway T-junction
RE09A-J	Serpentinised ultramafic	Open cut N of Melba Flat
RE10A-E	No. 2 dolomite and ore	South Stebbins 2050
RE11A	Dalcoath member	Howard 2035
RE11B-C	No. 3 ore	" "
RE12A-C	Federal ore	Federal 2000
RE13A-B	Melba ore	Melba 2015
RE13C	Mineralised RBM	" "
RE14A	Dolerite	R44
RE14B,D	Red Rock Member	"
RE14C	Dolerite	"
RE14E	Mineralised RRM	"
RE15A-D	No. 3 ore	S.A.2
RE16A-B	Red Rock member	300m down from 2 adit
RE16C	No. 2 dolomite	"

TABLE 2 MAGNETIC PROPERTIES

Sample	k	J	Q
RE01A	3	1	0.53
RE01B	2	1	0.79
RE01C	240	7,450	49
RE02A	170	6,210	58
RE02B	130	590	7.2
RE02C	150	2,990	32
RE02D	170	1,760	16
RE03A	37	1	0.04
RE04A	36	3	0.13
RE05A	24	1	0.07
RE05B	16	<1	<0.1
RE06A	49	1	0.03
RE06B	45	40	1.4
RE07A	5,330	3,400	1.0
RE07B	7,890	62,000	12
RE07C	6,360	3,150	0.79
RE08A	50	1	0.03
RE08B	69	8	0.18
RE08C	59	2	0.05
RE08D	30	2	0.11
RE09A	13,930	40,780	4.7
RE09B	3,350	1,560	0.74
RE09C	900	340	0.60
RE09D	2,570	2,090	1.3
RE09E	1,610	1,850	1.8
RE09F	3,210	1,470	0.73
RE09G	2,500	1,580	0.63
RE09H	2,800	11,100	6.3
RE09I	3,950	9,890	4.0
RE09J	920	1,030	1.8
RE10A	270	83	0.49
RE10B	120	170	2.3

Sample	k	J	Q
RE10C	2,900	2,380	1.3
RE10D	4,210	5,260	2.0
RE10E	140	87	1.0
RE11A	1,800	7,340	6.5
RE11B	3130	4,180	2.1
RE11C	3,390	3,420	2.1
RE12A	3,900	6,140	2.5
RE12B	18,970	111,800	9.4
RE12C	11,880	36,200	4.8
RE13A	5,010	4,690	1.5
RE13B	10,760	19,700	2.9
RE13C	2,640	2,520	1.5
RE14A	90	230	4.1
RE14B	34	3	0.14
RE14C	240	2,720	18
RE14D	92	97	1.7
RE14E	7,120	8,300	1.9
RE15A	11,610	6,500	0.89
RE15B	4,890	3,790	1.2
RE15C	3,730	2,850	1.2
RE15D	6,970	3,610	0.82
RE16A	24	1	0.07
RE16B	35	1	0.05
RE16C	23	1	0.14

k = CGS EMU susceptibility x 10^6

J = NRM intensity in microgauss (10 microgauss = 1 gamma)

Q = Koenigsberger ratio = J/kH, H = 0.63 oersteds

TABLE 3. NRM DIRECTIONS

Sample	NRM Direction (Dec, Inc)	Sample	NRM Direction (Dec, Inc)
RE01A	94°, - 55°	10A	144°, - 17°
1B	72°, - 57°	10B	10°, - 69°
1C	257°, - 22°	10C	352°, - 63°
		10D	13°, - 69°
2A	262°, - 62°	10E	158°, - 80°
2B	201°, + 16°		
2C	248°, - 58°	11A	101°, - 61°
2D	196°, + 33°	11B	2°, - 20°
		11C	92°, + 1°
3A	185°, - 76°		
		12A	290°, - 78°
4A	136°, + 19°	12B	189°, - 50°
		12C	191°, - 55°
5A	75°, + 64°		
5B	314°, - 40°	13A	42°, - 70°
		13B	62°, - 70°
6A	336°, - 58°	13C	256°, - 82°
6B	346°, - 39°		
		14A	326°, - 81°
7A	25°, - 21°	14B	27°, - 71°
7B	262°, - 19°	14C	313°, - 83°
7C	27°, - 32°	14D	194°, - 33°
		14E	234°, - 67°
8A	353°, - 60°		
8B	3°, - 68°	15A	102°, - 30°
8C	353°, - 53°	15B	221°, - 38°
8D	336°, - 66°	15C	128°, - 28°
9A	176°, - 52°	15D	97°, - 49°
9B	3°, - 38°		
9C	9°, - 40°	16A	330°, - 71°
9D	337°, - 69°	16B	303°, - 74°
9E	5°, - 74°	16C	42°, - 77°
9F	354°, - 39°		
9G	347°, - 69°		
9H	109°, - 15°		
9I	97°, - 11°		
9J	70°, - 56°		

TABLE 4. PALAEOMAGNETIC DIRECTIONS AND POLE POSITIONS

Rock type	Formation mean direction		N	K	α_{95}	Pole		dp	dm
	Dec.	Inc.				Lat.	Long.		
Sediments + spilites	335°	-74°	7	18.9	14°	66°S	176°E	23°	25°
Ultramafics	020°	-21°	9	10.6	17°	55°S	001°E	9°	18°
Sulphide ores	228°	-74°	14	11.2	12°	18°S	169°E	20°	22°

N = no. of specimen directions included in mean

K = estimate of Fisherian precision parameter

α_{95} = Half-angle of 95% cone of confidence about mean direction

dp = semi-axis along palaeomeridian of 95% oval of confidence about pole

dm = semi-axis of 95% oval of confidence about pole, orthogonal to palaeomeridian

TABLE 5. SUSCEPTIBILITY ANISOTROPY

Sample	$\bar{k}$	$\bar{A}$	$\bar{L}$	$\bar{F}$	$\bar{P}$
1A	3	1.03	1.02	1.01	1.01
1B	2	1.02	1.01	1.01	1.00
1C	240	1.16	1.05	1.10	0.96
2A	165	1.10	1.07	1.03	1.04
2B	130	1.04	1.03	1.01	1.02
2C	145	1.04	1.03	1.01	1.01
2D	165	1.04	1.02	1.02	1.00
3A	37	1.01	1.00	1.01	0.99
4A	36	1.00	1.00	1.00	1.00
5A	24	1.00	1.00	1.00	1.00
5B	16	1.01	1.00	1.01	0.99
6A	49	1.01	1.01	1.00	1.01
6B	45	1.01	1.01	1.00	1.01
7A	5330	1.40	1.05	1.34	0.78
7B	8300	1.31	1.03	1.27	0.81
7C	6530	1.26	1.02	1.24	0.82
8A	50	1.02	1.01	1.01	1.00
8B	69	1.02	1.01	1.01	1.00
8C	59	1.02	1.01	1.01	1.00
8D	30	1.02	1.01	1.01	1.00
9A	11800	1.88	1.06	1.79	0.59
9B	3350	1.11	1.07	1.04	1.02
9C	900	1.22	1.10	1.11	1.00
9D	2570	1.33	1.00	1.32	0.76
9E	1610	1.24	1.04	1.19	0.87
9F	3180	1.14	1.05	1.09	0.97
9G	2440	1.20	1.03	1.18	0.89
9H	2790	1.16	1.04	1.12	0.94
9I	4135	1.19	1.06	1.12	0.94
9J	960	1.10	1.05	1.04	1.01
10A	270	1.09	1.02	1.07	0.96
10B	120	1.26	1.09	1.16	0.94
10C	3310	1.62	1.13	1.44	0.79
10D	6820	2.33	1.37	1.70	0.81
10E	140	1.14	1.09	1.05	1.04
11A	2020	1.56	1.11	1.40	0.81
11B	1990	1.57	1.13	1.38	0.85
11C	3580	1.36	1.17	1.16	1.01

Sample	$\bar{k}$	$\bar{A}$	$\bar{L}$	$\bar{F}$	$\bar{P}$
12A	4600	1.72	1.17	1.47	0.84
12B	21400	2.18	1.12	1.96	0.59
12C	19980	2.32	1.15	2.02	0.60
13A	4590	1.53	1.26	1.21	1.05
13B	10710	1.39	1.15	1.21	0.95
13C	2930	1.33	1.17	1.14	1.04
14A	90	1.03	1.02	1.01	1.01
14B	34	1.06	1.04	1.02	1.02
14C	240	1.05	1.03	1.02	1.01
14D	86	1.29	1.17	1.11	1.06
14E	7320	1.45	1.17	1.23	0.96
15A	9180	2.46	1.27	1.94	0.67
15B	3770	-	-	-	-
15C	2940	-	-	-	-
15D	5830	-	-	-	-
16A	24	1.03	1.01	1.01	1.00
16B	35	1.02	1.01	1.01	1.00
16C	23	1.02	1.01	1.01	1.01

k = bulk susceptibility = $(k_1 + k_2 + k_3)/3$

A = anisotropy ratio = k_1/k_3

L = magnetic lineation ratio = k_1/k_2

F = magnetic foliation ratio = k_2/k_3

P = prolateness of susceptibility ellipsoid = L/F

Arithmetic means are denoted by $\bar{A}$ etc.

TABLE 6. MAGNETIC FABRIC

Sample(s)	Magnetic lineation			Magnetic foliation pole		
	Dec (°)	Inc(°)	(α_{95})	Dec(°)	Inc(°)	(α_{95})
1A		No distinct fabric				
1B		"				
1C	184	+13	(55)	96	+9	(-)
2A-D	192	+65	(10)			
3A	78	+42	(17)	275	+46	(9)
4A		No distinct fabric				
5A-B	149	+77	(20)			
6A-B	181	+10	(18)	295	+59	(31)
7A-C	149	+62	(10)	340	+28	(11)
8A-D	132	+70	(21)	294	+16	(20)
9A-G		Fabric very confused				
9H	104	+10	(16)	196	+10	(13)
9I	145	+57	(22)	237	-1	(21)
9J	124	+12	(-)	219	+21	(-)
10A	203	+48	(31)	92	+20	(23)
10B	192	+11	(32)	98	+41	(43)
10C				133	+80	(14)
10D	89	+12	(7)	277	+78	(6)
10E	324	+40	(11)	73	+22	(22)
11A	358	+6	(17)	92	+38	(28)
11B	51	+13	(25)	154	+54	(16)
11C	118	+16	(23)	243	+57	(32)
12A	142	+5	(21)	231	+16	(31)
12B	137	+34	(7)	253	+33	(9)
12C	103	+52	(15)	222	+20	(6)
13A	168	+15	(22)	334	+70	(16)
13B		Fabric confused				
13C	41	+24	(26)	244	+64	(23)
14A,C	146	+72	(16)	54	+1	(14)
14B,D	33	+8	(22)	273	+69	(26)
14E	73	+38	(26)	265	+54	(30)
15A	267	+10	(9)	151	+68	(9)
15B	252	+8	(25)	133	+73	(16)
15C	7	+3	(21)	116	+78	(12)
15D		-			-	
16A	274	0	(24)	1	+85	(21)
16B	24	+29	(36)	223	+54	(25)
16C	181	+17	(28)	86	+14	(18)

Fig. 1 (a) NRM directions of sediment and spilite samples from sites 3,5,6,8,14 and 16.

(b) NRM directions of ultramafic samples from sites 7 and 9.

Open and closed symbols denote upward-pointing and downward-pointing directions respectively. Circles indicate NRM directions, the square indicates the mean NRM direction with the 95% cone of confidence shown dashed. Outlying directions are indicated by crossed circles and are excluded from the calculation of the mean. DF = dipole field direction, PF = present field direction. Stereographic projection with the primitive representing the present horizontal.

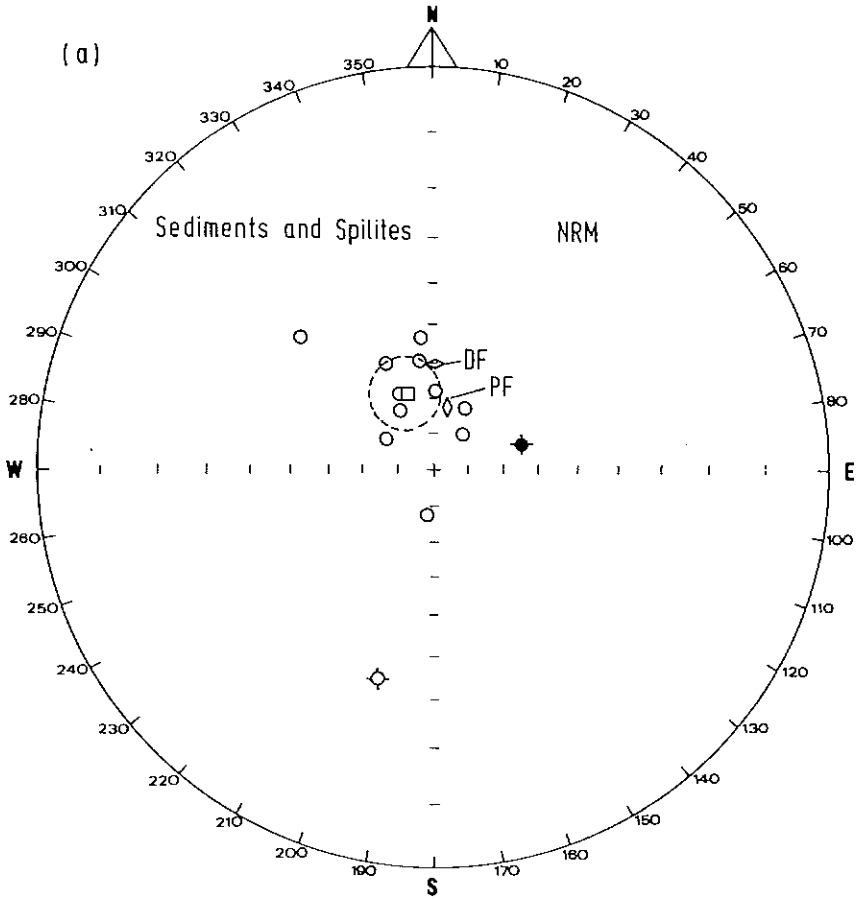
(a)
N
S
W
E
Sediments and Spilites
NRM
DF
PF

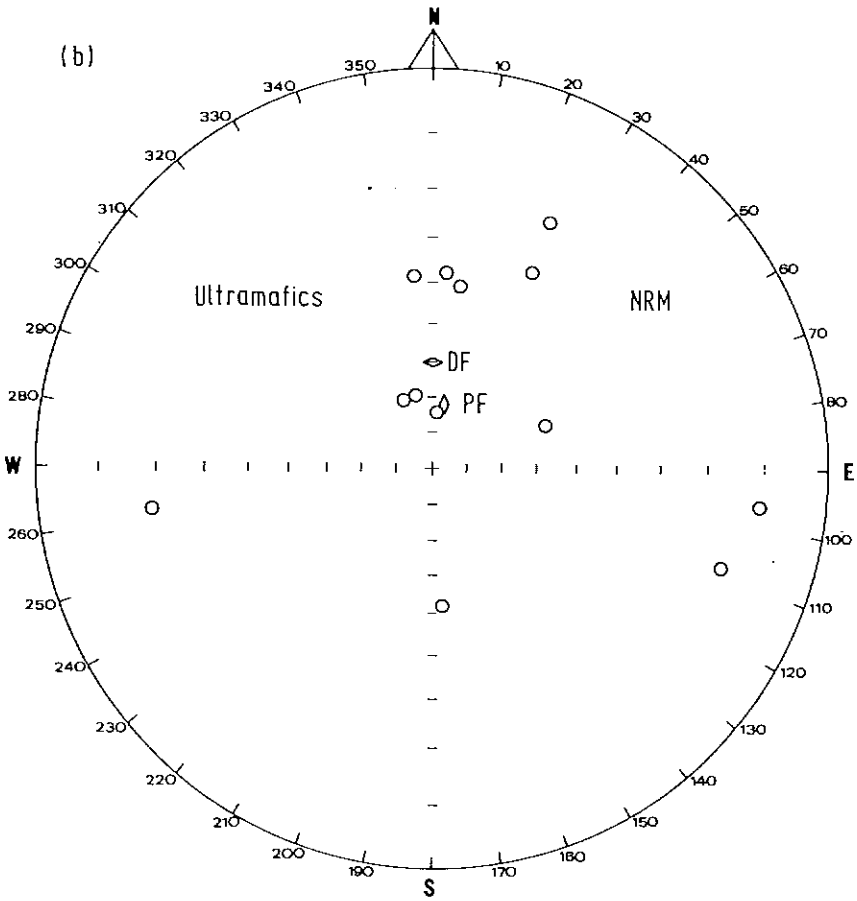
(b)
N
S
W
E
Ultramafics
NRM
DF
PF

Fig. 1

Fig. 2. NRM directions of mineralised samples from sites 10, 11, 12, 13, 14 and 15. Symbols as for Fig. 1

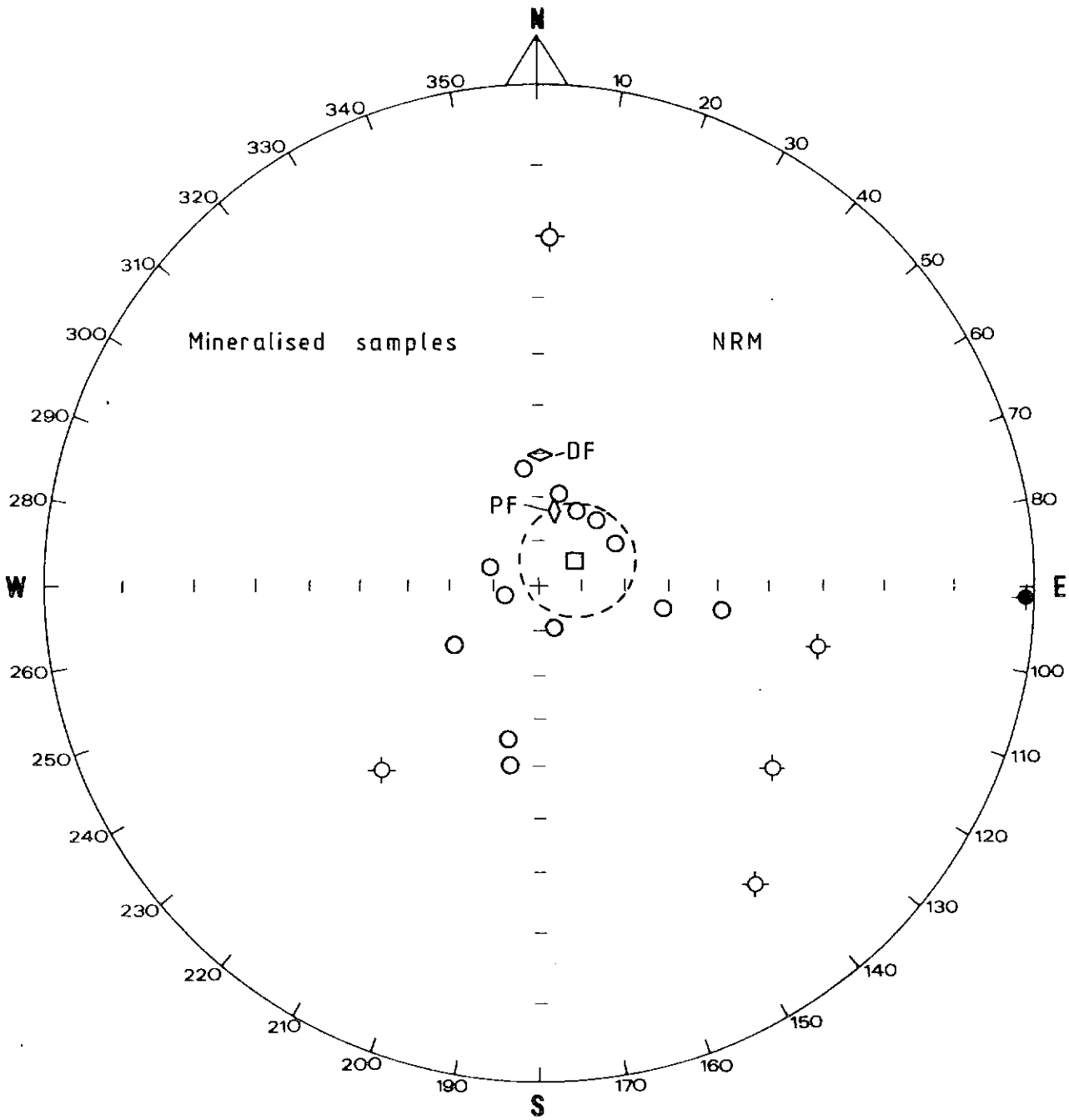
N
S
E
W
10
20
30
40
50
60
70
80
100
110
120
130
140
150160
170
190
200
210
220
230
240
250
260
280
290
300
310
320
330
340
350
Mineralised samples
NRM
DF
PF

Fig. 2

Fig. 3. Low field thermomagnetic (k-T) curves for (a) RE09D, (b) REIOD. Heating and cooling curves are distinguished by arrows. In (b) the reversibility of the curve was tested by cooling from ~270°C. An alternative curve obtained if the initial heating is continued is shown dashed. The Curie temperature (T_C) is indicated.

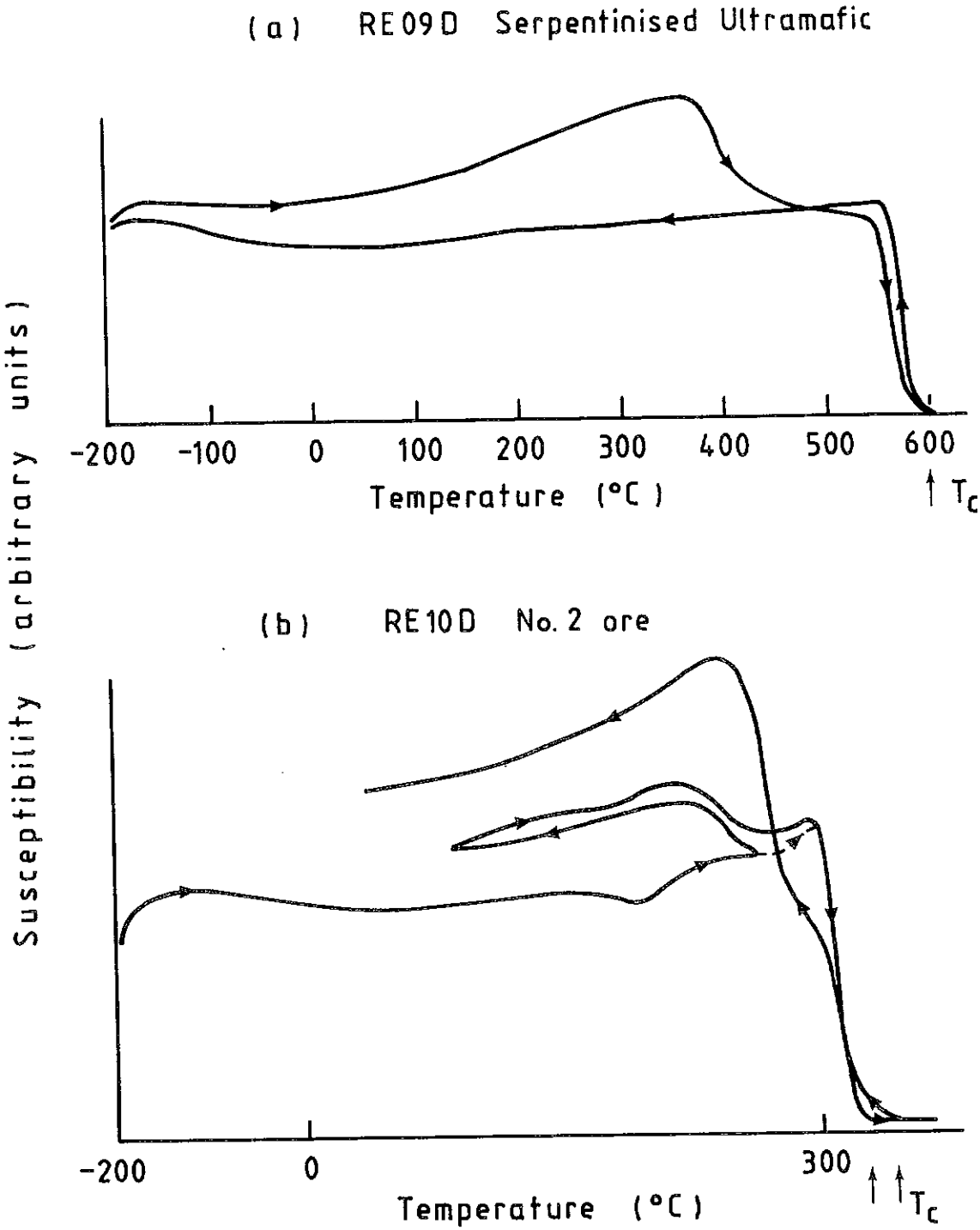
(a) RE09D Serpentinised Ultramafic
Susceptibility (arbitrary units)
-200
-100
0
100
200
300
400
500
600
Temperature (°C)
T_c
(b) RE10D No. 2 ore
-200
0
300
Temperature (°C)
T_c

Fig. 3

Fig. 4. k-T curves for (a) RE11B, (b) RE12A, (c) RE13B

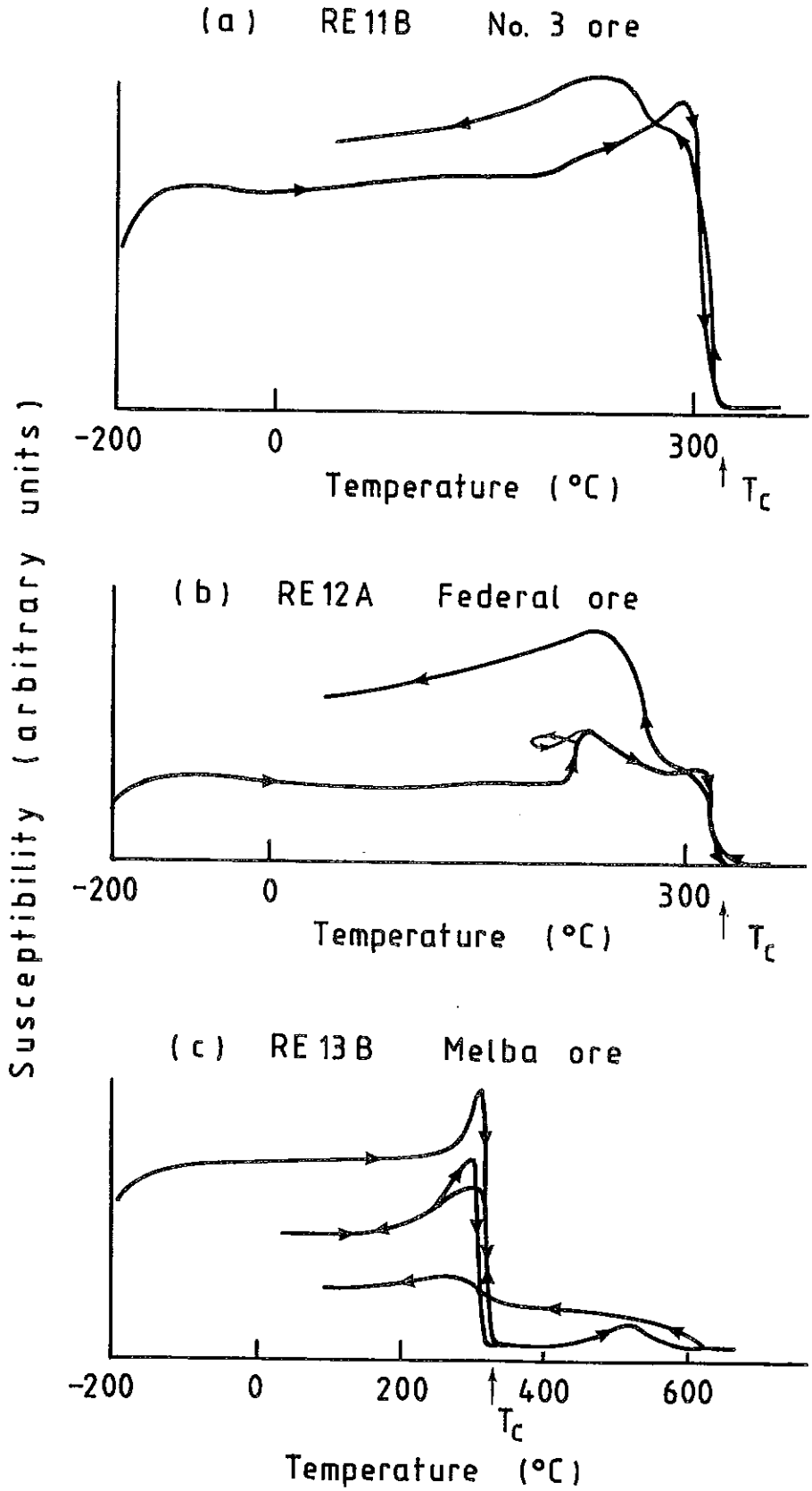
(a) RE11B No. 3 ore
-200
0
300
Tc
Temperature (°C)
(b) RE12A Federal ore
-200
0
300
Tc
Temperature (°C)
(c) RE13B Melba ore
-200
0
200
400
600
Tc
Temperature (°C)
Susceptibility (arbitrary units)

Fig. 4

Fig. 5. k-T curves for (a) RE14E, (b) RE15B

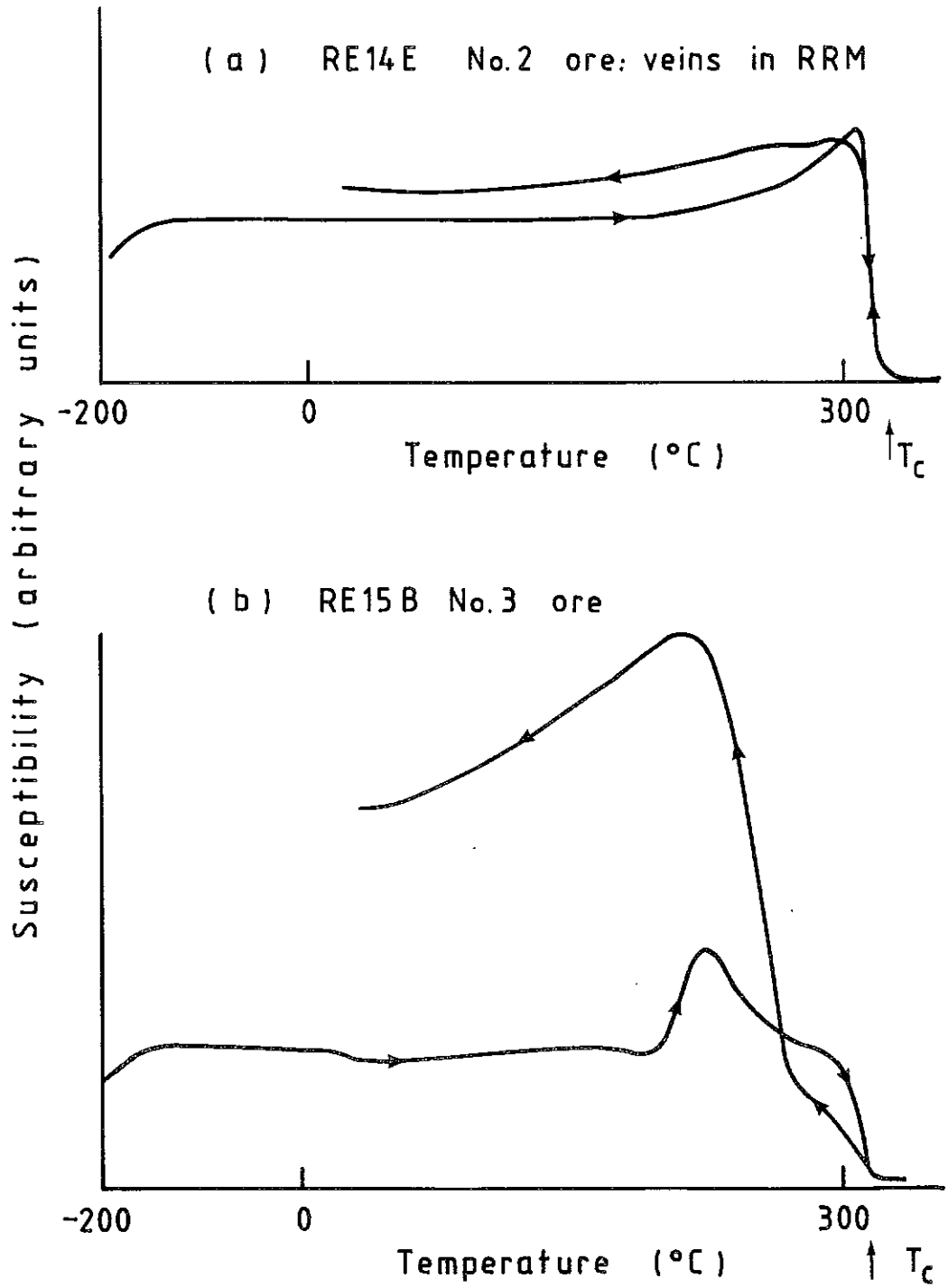
(a) RE14E No.2 ore: veins in RRM
Susceptibility (arbitrary units)
-200
0
300
Temperature (°C)
T_c
(b) RE15B No.3 ore
Susceptibility (arbitrary units)
-200
0
300
Temperature (°C)
T_c

Fig. 5

Fig. 6. Vector diagrams for thermal demagnetisation of gabbro specimens (a) RE02A1, (b) RE02B1, (c) RE02C1, (d) RE02D1. Symbols joined by lines indicate projections of end-points of remanence vectors measured after successive demagnetisation steps. Crosses represent projections of vectors onto the horizontal plane, circles represent projections onto the indicated vertical plane (either E-W as in (a) or N-S as in (b)). Steps shown are NRM, 200°, 300°, 350°, 400°, 450°, 500°, 550°.

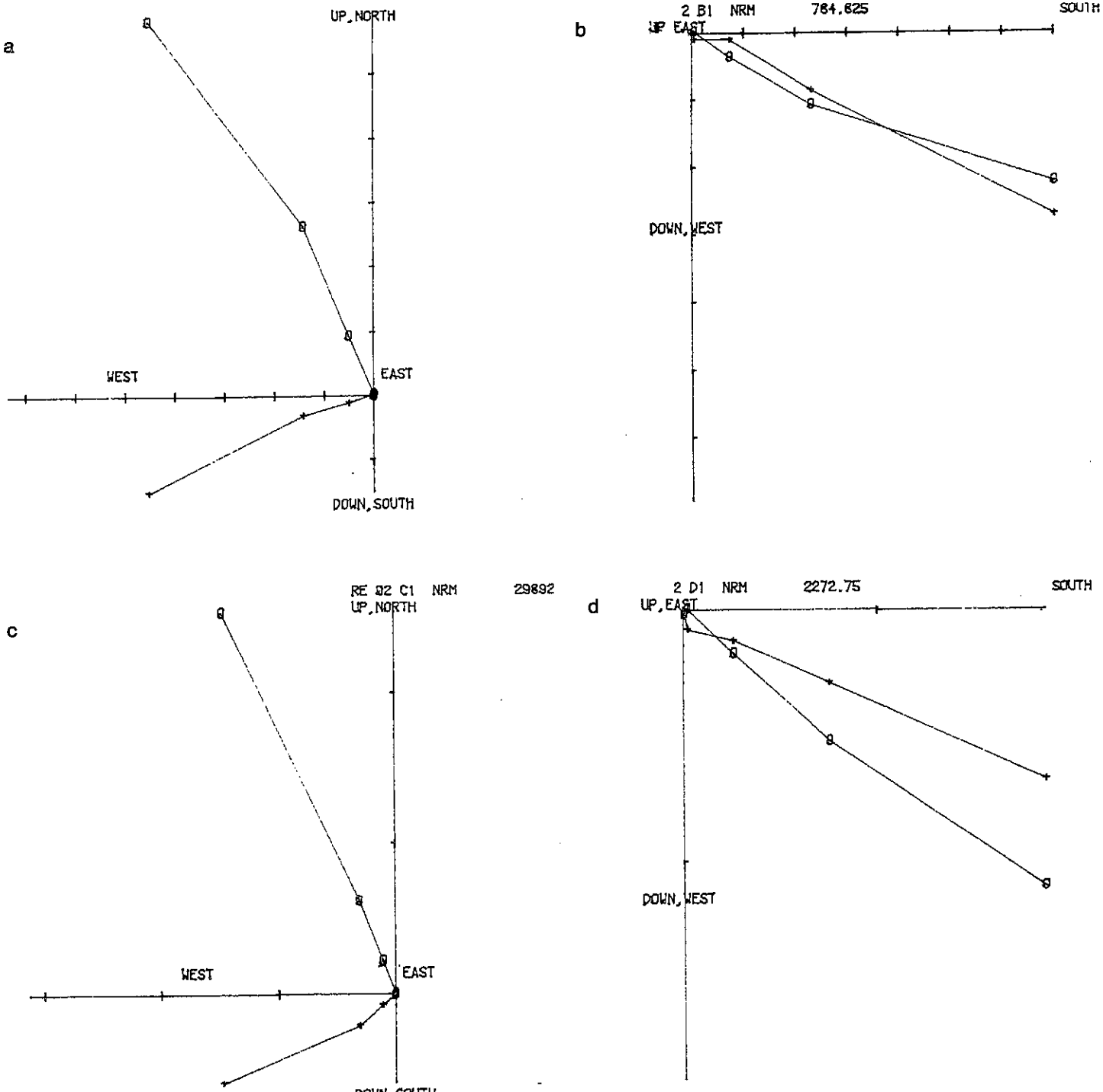
a
UP, NORTH
WEST
EAST
DOWN, SOUTH
b
2 B1 NRM 764.625
SOUTH
UP EAST
DOWN, WEST
c
RE 02 C1 NRM 29892
UP, NORTH
WEST
EAST
DOWN, SOUTH
d
2 D1 NRM 2272.75
SOUTH
UP, EAST
DOWN, WEST

FIG.6

Fig. 7 Vector plots for AF and thermal palaeomagnetic cleaning of ultramafic specimens (a) RE07A (NRM, 200°, 300°, 350°, 400°, 450°, 500°, 550°, 570°), (b) RE09A1 (NRM, 10oe, 20oe, 50oe, 100oe, 150oe, 200oe, 300oe, 400oe, 500oe, 650oe, 800oe, 1000oe), (c) RE0931 (steps as for (a)), (d) RE09D (NRM, 25oe, 50oe, 75oe, 100oe, 150oe, 200oe, 400oe, 600oe, 800oe, 1000oe).

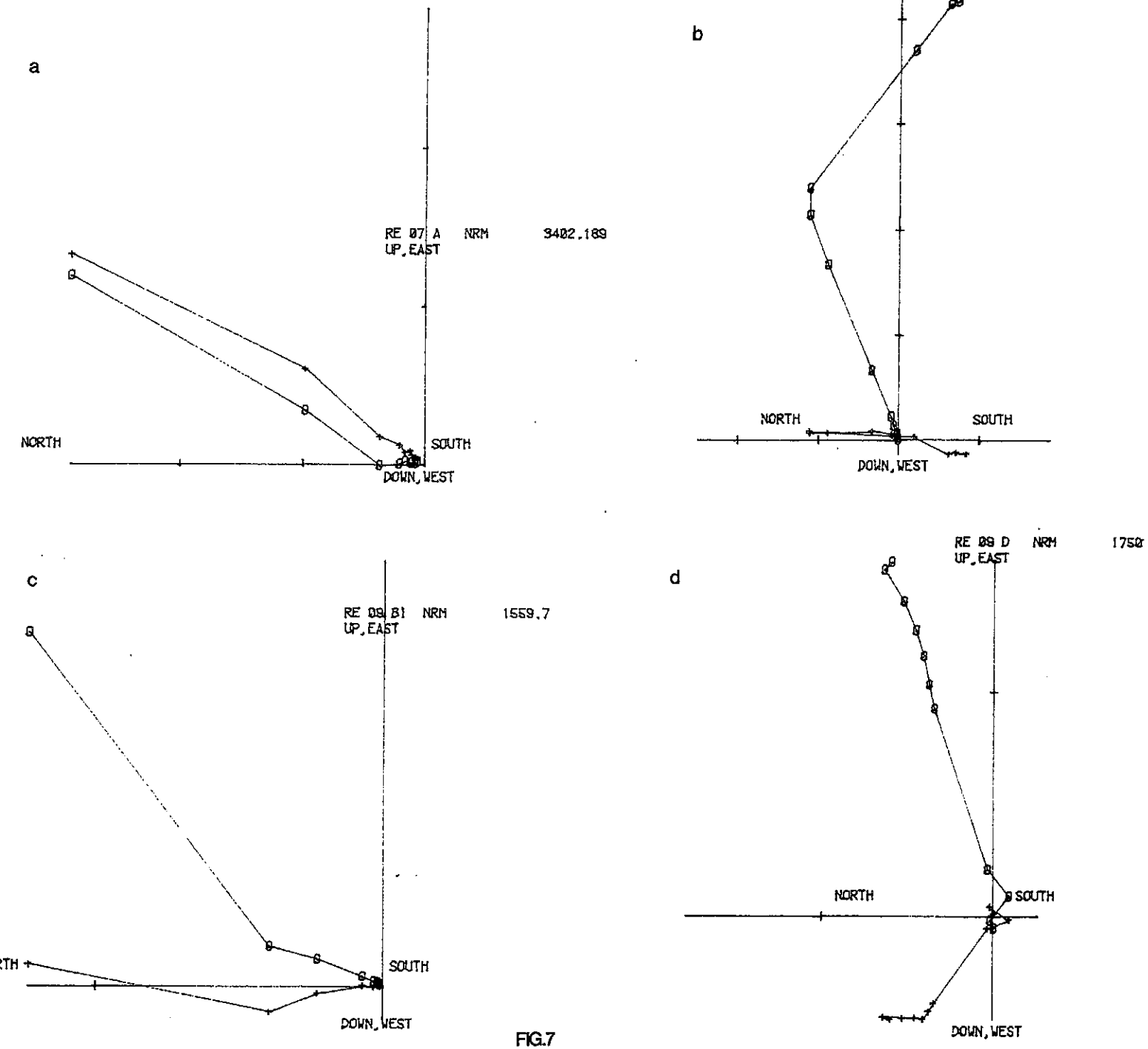
a
RE 07 A NRM 3402.189
UP, EAST
NORTH
SOUTH
DOWN, WEST
b
re 09 a1 nrm 43187.5
UP, EAST
NORTH
SOUTH
DOWN, WEST
c
RE 09 B1 NRM 1559.7
UP, EAST
NORTH
SOUTH
DOWN, WEST
d
RE 09 D NRM 1750
UP, EAST
NORTH
SOUTH
DOWN, WEST

FIG.7

Fig. 8. Vector plots for AF and thermal demagnetisation of mineralised specimens from site 10 (a) RE10C3 (AF to 400oe), (b) RE10D3 (AF to 400 oe), (c) RE10D1 (thermal to 330°C), (d) RE10E1 (thermal to 310°C). The standard thermal demagnetisation steps for sulphide ores were NRM, 100°, 130°, 160°, 190°, 220°, 250°, 270°, 290°, 300°, 310°, 320°, 330°.

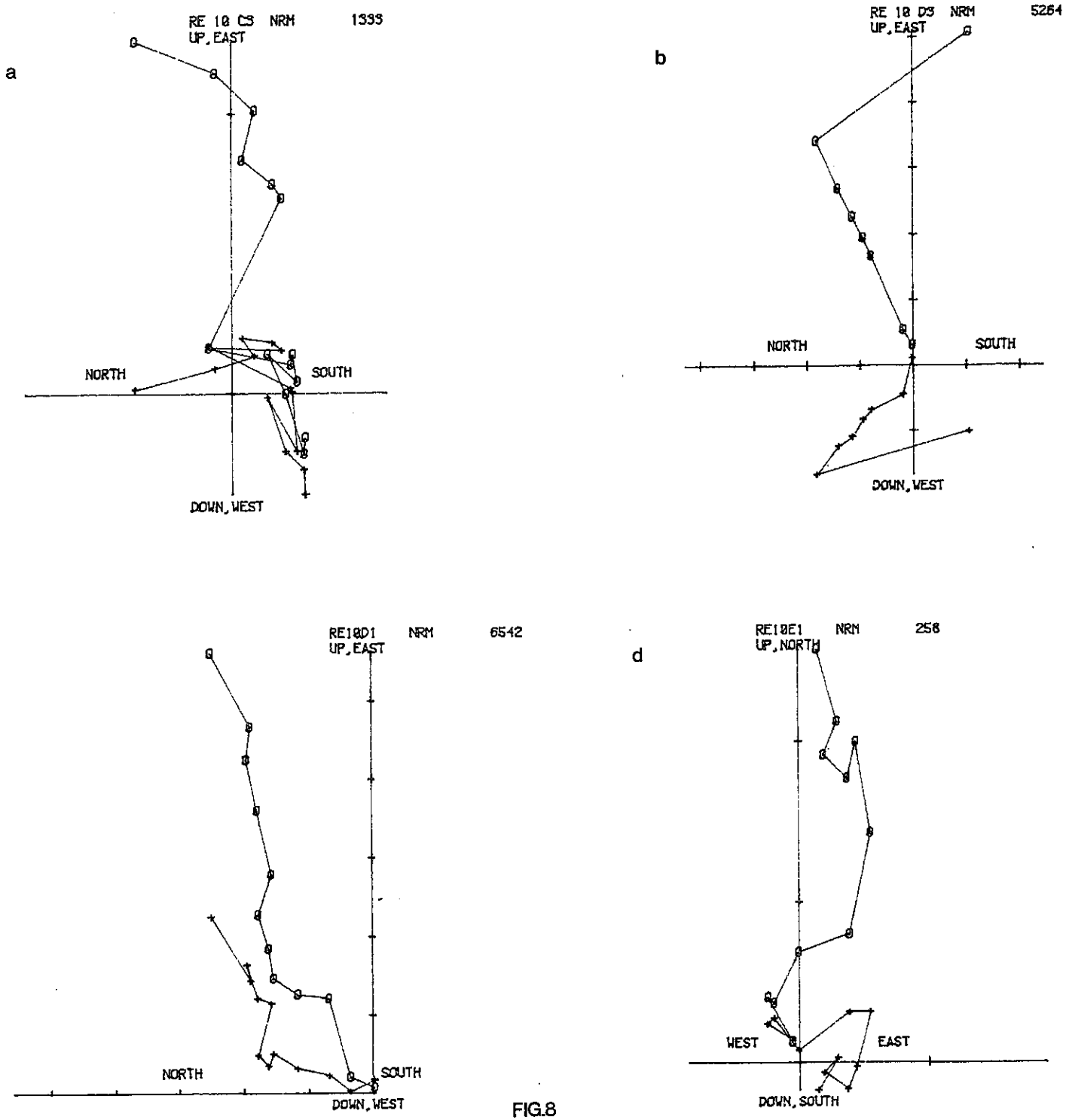
a
RE 10 C3 NRM 1333
UP, EAST
NORTH
SOUTH
DOWN, WEST
b
RE 10 D3 NRM 5264
UP, EAST
NORTH
SOUTH
DOWN, WEST
c
RE10D1 NRM 6542
UP, EAST
NORTH
SOUTH
DOWN, WEST
d
RE10E1 NRM 258
UP, NORTH
WEST
EAST
DOWN, SOUTH

FIG.8

Fig. 9. Vector plots for AF and thermal demagnetisation of Federal ore specimens (a) RE12A1 (thermal to 310°), (b) RE12A4 (AF to 100oe), (c) RE12B1 (AF to 200oe), (d) RE12C2 (AF to 200 oe).

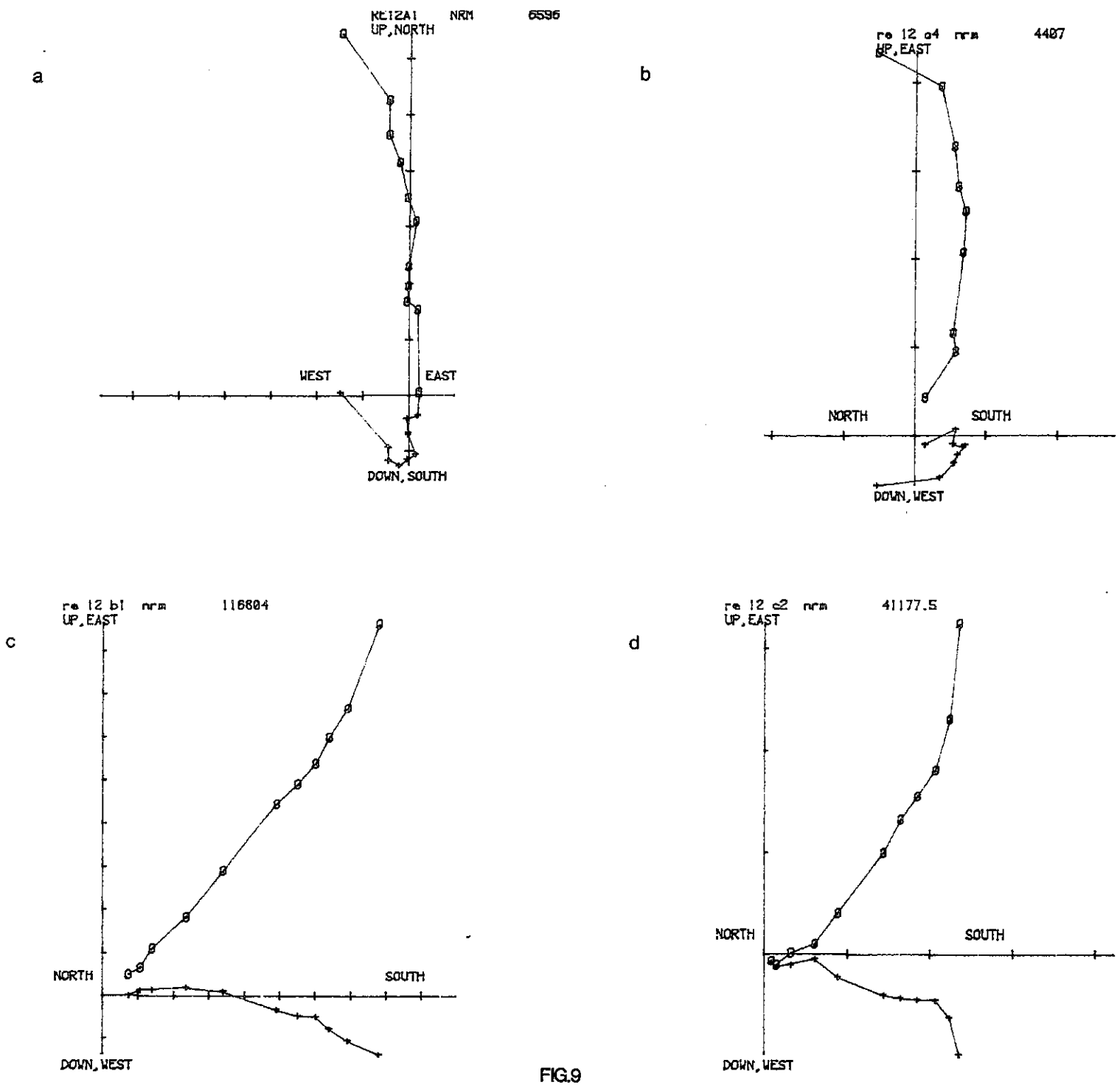
a
KE12A1 NRM 6596
UP, NORTH
WEST
EAST
DOWN, SOUTH
b
re 12 a4 nrm 4407
UP, EAST
NORTH
SOUTH
DOWN, WEST
c
re 12 b1 nrm 116804
UP, EAST
NORTH
SOUTH
DOWN, WEST
d
re 12 c2 nrm 41177.5
UP, EAST
NORTH
SOUTH
DOWN, WEST

FIG.9

Fig. 10. Vector plots for AF and thermal demagnetisation of Melba ore specimens (a) RE13A2 (thermal to 310°), (b) RE13B3 (thermal to 310°) (c) RE13B2 (AF to 150oe), (d) RE13C1 (AF to 75oe).

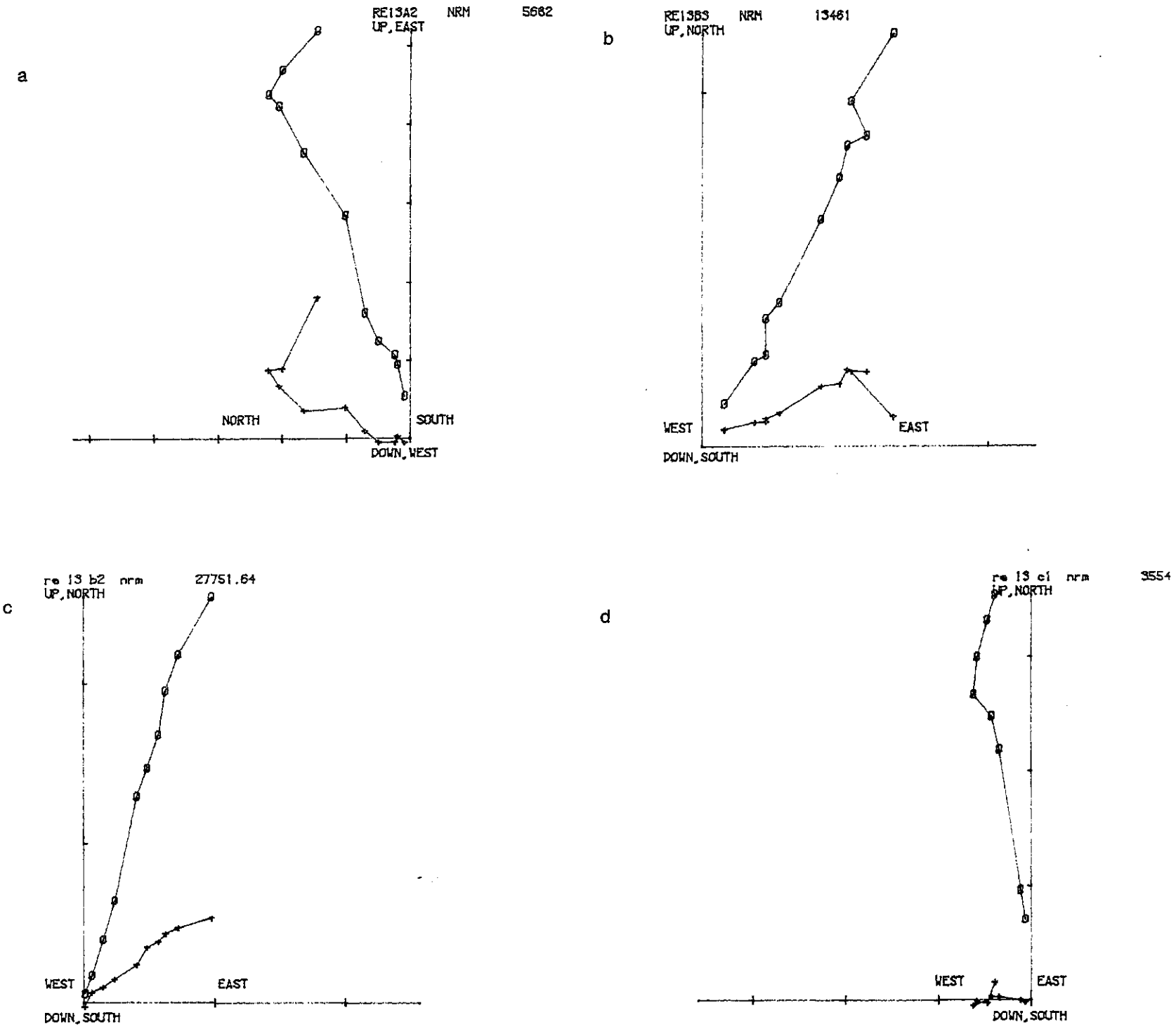
a
RE13A2 NRM 5682
UP, EAST
NORTH
SOUTH
DOWN, WEST
b
RE13B3 NRM 13461
UP, NORTH
WEST
EAST
DOWN, SOUTH
c
re 13 b2 nrm 27751.64
UP, NORTH
WEST
EAST
DOWN, SOUTH
d
re 13 c1 nrm 3554
UP, NORTH
WEST
EAST
DOWN, SOUTH

FIG. 10

Fig. 11. Vector plots for AF and thermal demagnetisation of specimens from site 14 (a) RE14E2 (ore specimen, thermal to 330°), (b) RE14E4 (ore, AF to 140 oe), (c) RE14A1 (dolerite, thermal to 570°), (d) RE14C1 (dolerite, AF to 500 oe).

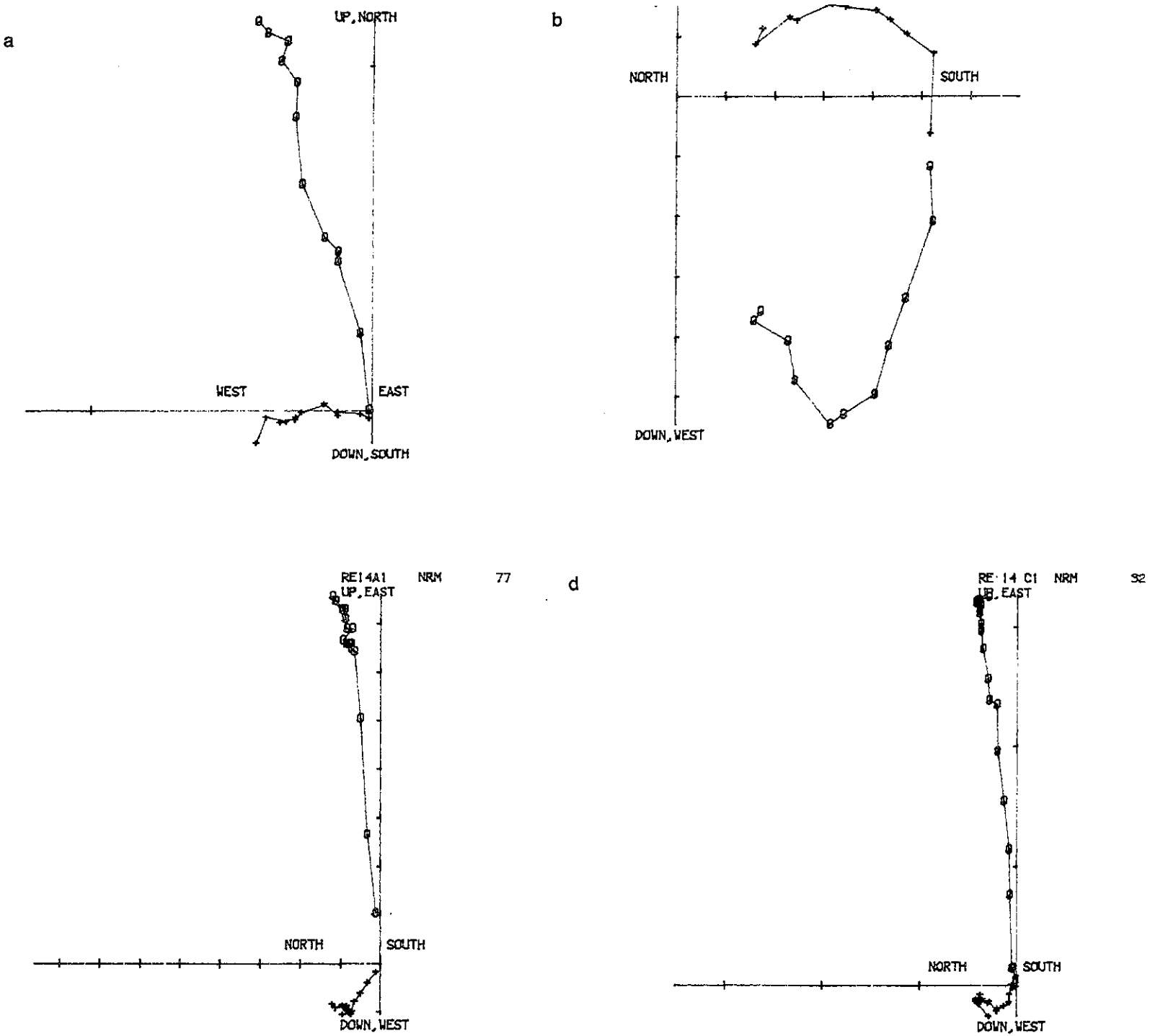
a
UP, NORTH
WEST
EAST
DOWN, SOUTH
b
NORTH
SOUTH
DOWN, WEST
c
RE14A1 NRM 77
UP, EAST
NORTH
SOUTH
DOWN, WEST
d
RE 14 C1 NRM 32
UP, EAST
NORTH
SOUTH
DOWN, WEST

FIG.11

Fig. 12. Vector plots for thermal demagnetisation to 330°C for ore specimens from sites 11 and 15 (a) RE11A1, (b) RE11B2, (c) RE11C1, (d) RE15A2.

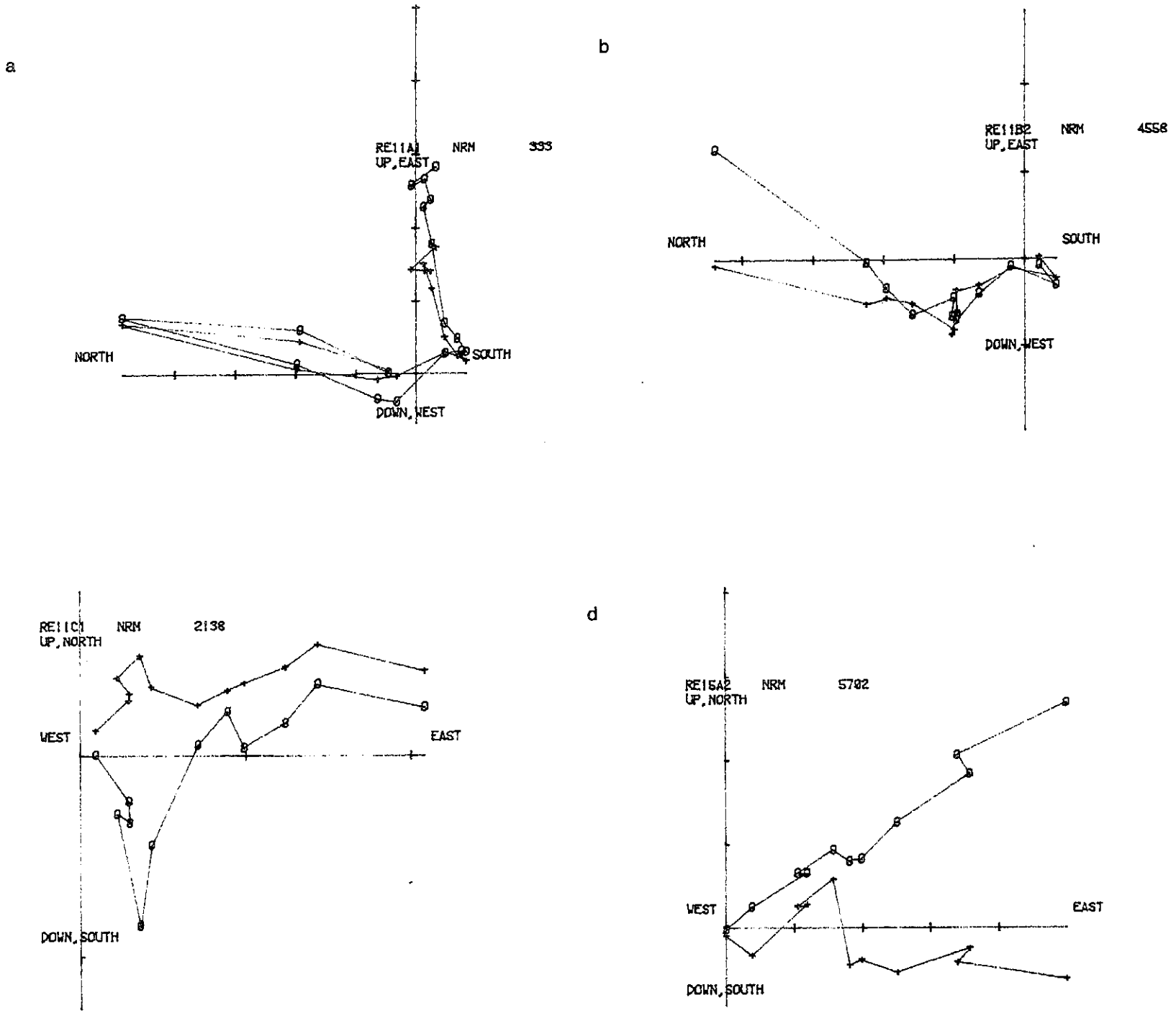
a
RE11A1 NRM 333
UP, EAST
NORTH
SOUTH
DOWN, WEST
b
RE11B2 NRM 4558
UP, EAST
NORTH
SOUTH
DOWN, WEST
c
RE11C1 NRM 2138
UP, NORTH
WEST
EAST
DOWN, SOUTH
d
RE15A2 NRM 5702
UP, NORTH
WEST
EAST
DOWN, SOUTH

FIG.12

Fig. 13. Vector plots for AF and thermal demagnetisation of ore specimens from site 15 (a) RE15A1 (AF to 120 oe), (b) RE15B3 (AF to 140 oe), (c) RE15C1 (thermal to 290°), (d) RE15D2 (thermal to 320°).

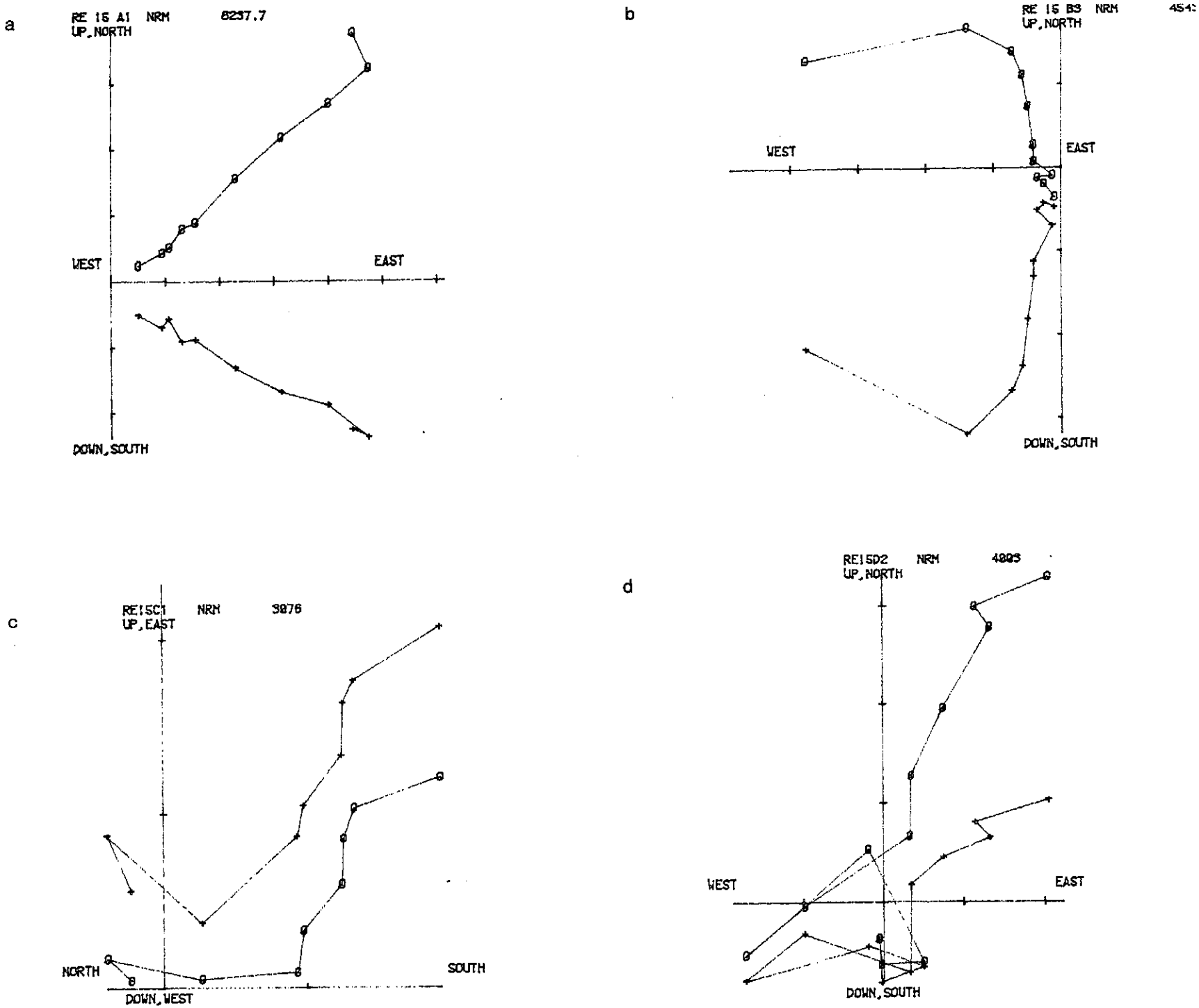
a
RE 15 A1 NRM 8237.7
UP, NORTH
WEST
EAST
DOWN, SOUTH
b
RE 15 B3 NRM
UP, NORTH
WEST
EAST
DOWN, SOUTH
c
RE15C1 NRM 3876
UP, EAST
NORTH
SOUTH
DOWN, WEST
d
RE15D2 NRM 4893
UP, NORTH
WEST
EAST
DOWN, SOUTH

FIG.13

Fig. 14. High temperature remanence components from sediment and spilite specimens. Symbols as in Fig. 1.

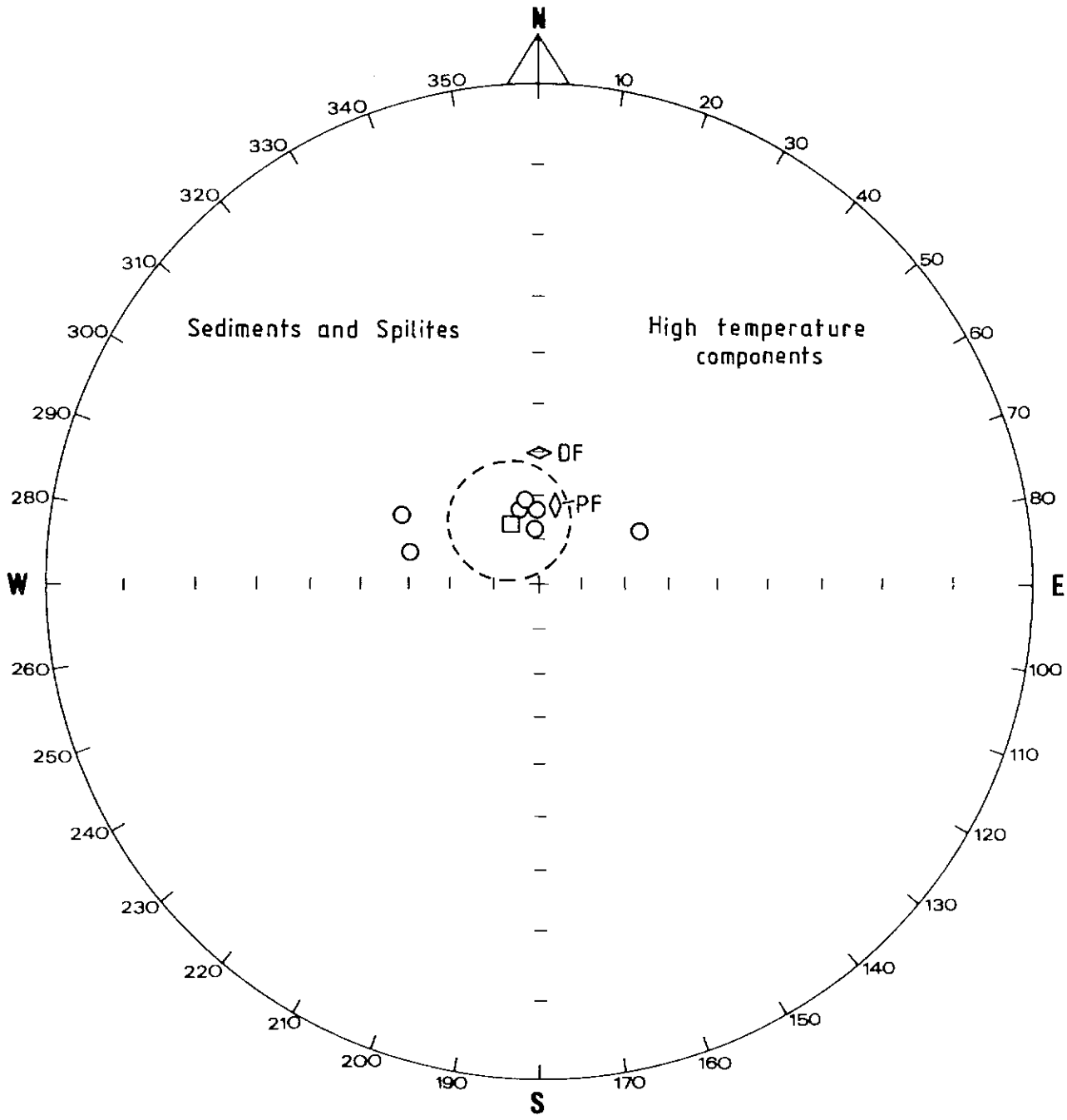
N
S
E
W
10
20
30
40
50
60
70
80
100
110
120
130
140
150
160
170
190
200
210
220
230
240
250
260
280
290
300
310
320
330
340
350
Sediments and Spilites
High temperature components
DF
PF

Fig. 14

Fig. 15. High temperature remanence components from ultramafic specimens. Symbols as in Fig. 1.

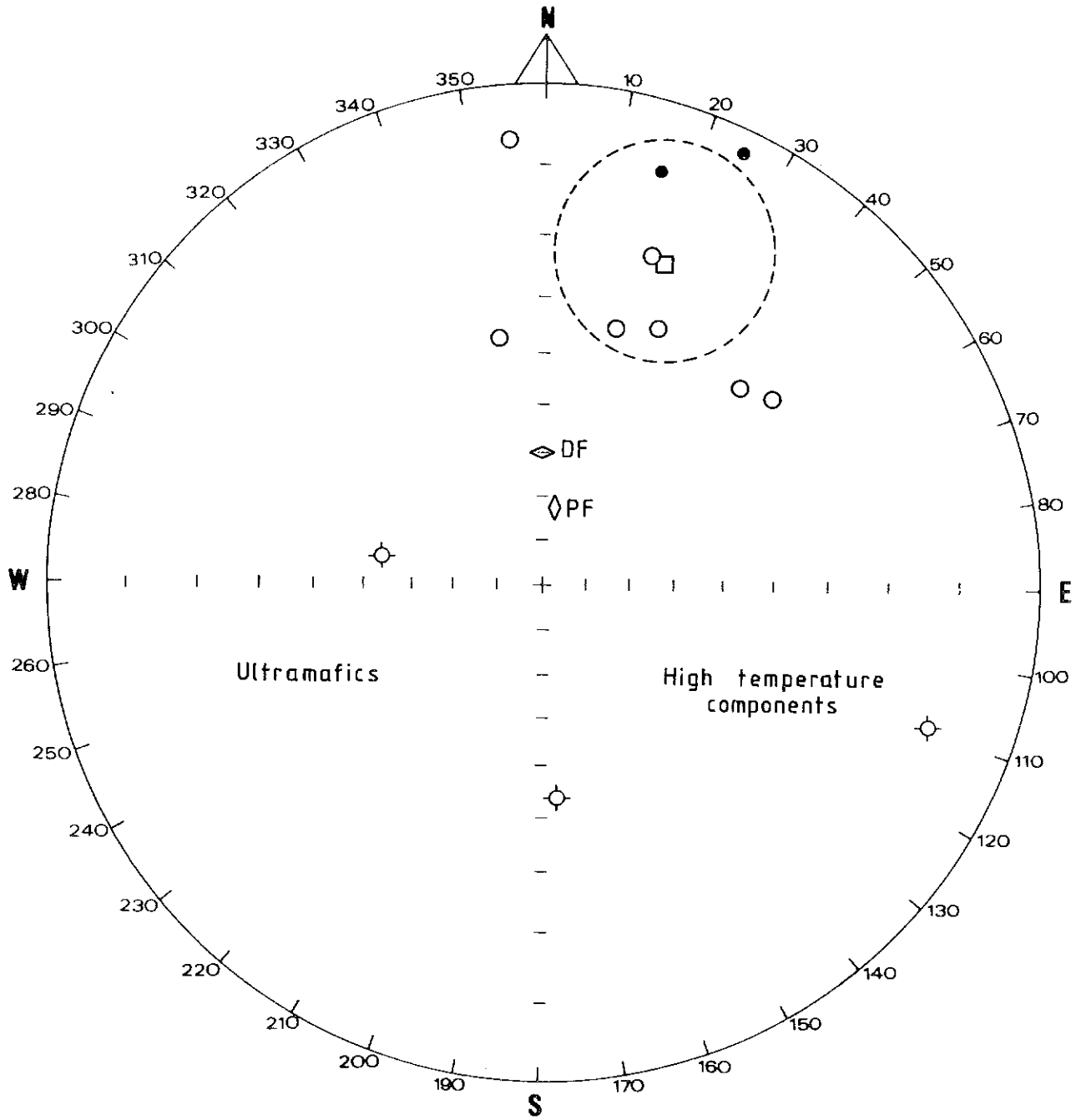
N
S
E
W
350
10
20
30
40
50
60
70
80
100
110
120
130
140
150
160
170
190
200
210
220
230
240
250
260
280
290
300
310
320
330
340
DF
PF
Ultramafics
High temperature components

Fig. 15

Fig. 16. High temperature remanence components from mineralised samples. Symbols as in Fig. 1.

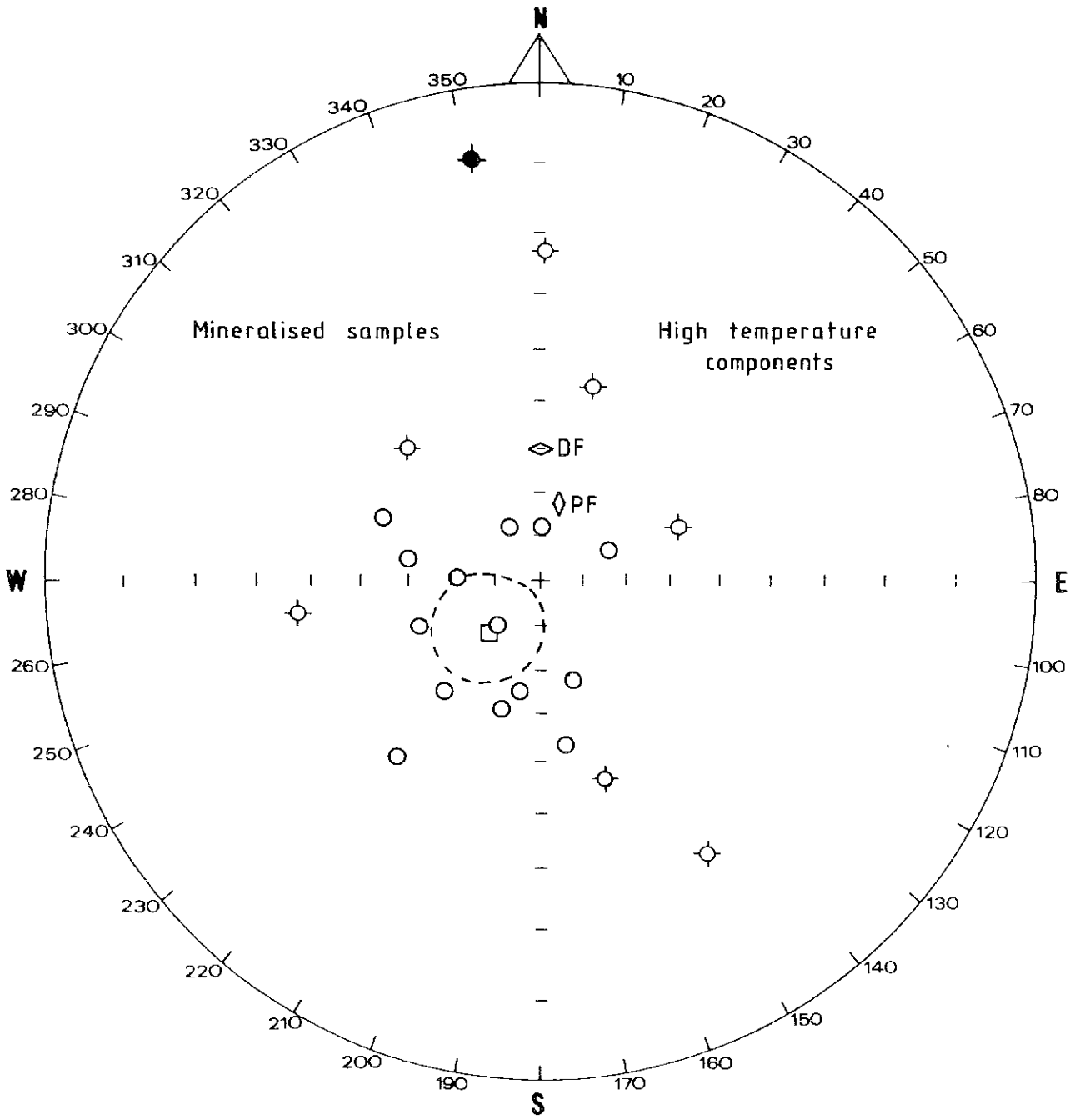
N
S
W
E
10
20
30
40
50
60
70
80
100
110
120
130
140
150
160
170
190
200
210
220
230
240
250
260
280
290
300
310
320
330
340
350
Mineralised samples
High temperature components
DF
PF

Fig. 16

Fig. 17. Magnetic fabric of specimens from (a) site 2, (b) site 3, (c) site 5, (d) site 6. Minor susceptibility axes (magnetic foliation poles) are indicated by dots, major susceptibility axes (magnetic lineations) by squares. The mean foliation pole (if well-defined) is indicated by an asterisk and the foliation plane is indicated by the orthogonal girdle. The mean lineation is indicated by a star. The circles around the mean directions are 95% cones of confidence. Stereographic lower hemisphere projection.

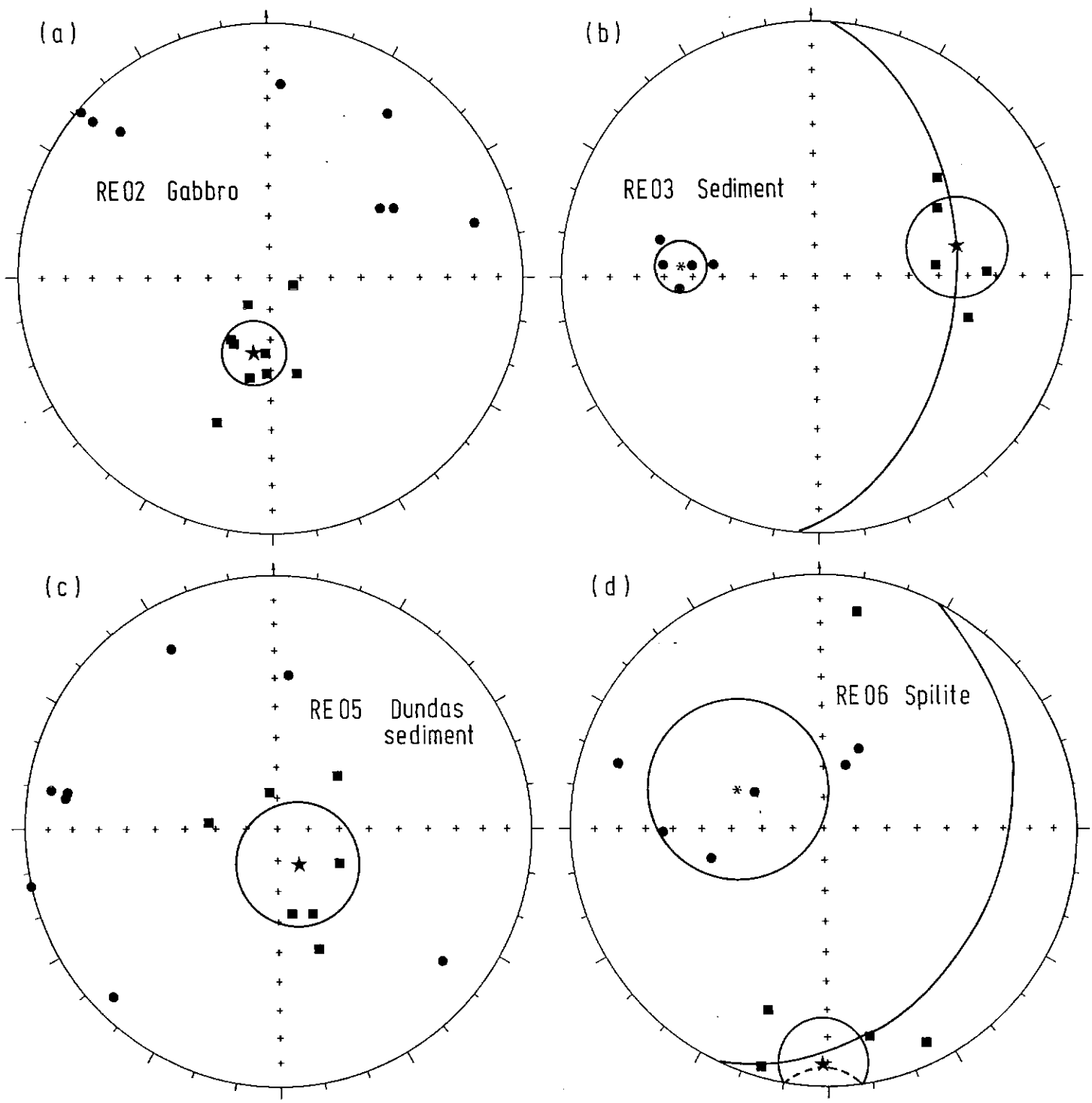
(a)
RE02 Gabbro
(b)
RE03 Sediment
(c)
RE05 Dundas sediment
(d)
RE06 Spilite

Fig. 17

Fig. 18. Magnetic fabric of (a) specimens from site 7 (b) specimens from site 8, (c) samples from site 9, (d) samples from the No.2 dolomite. Symbols as in Fig. 17.

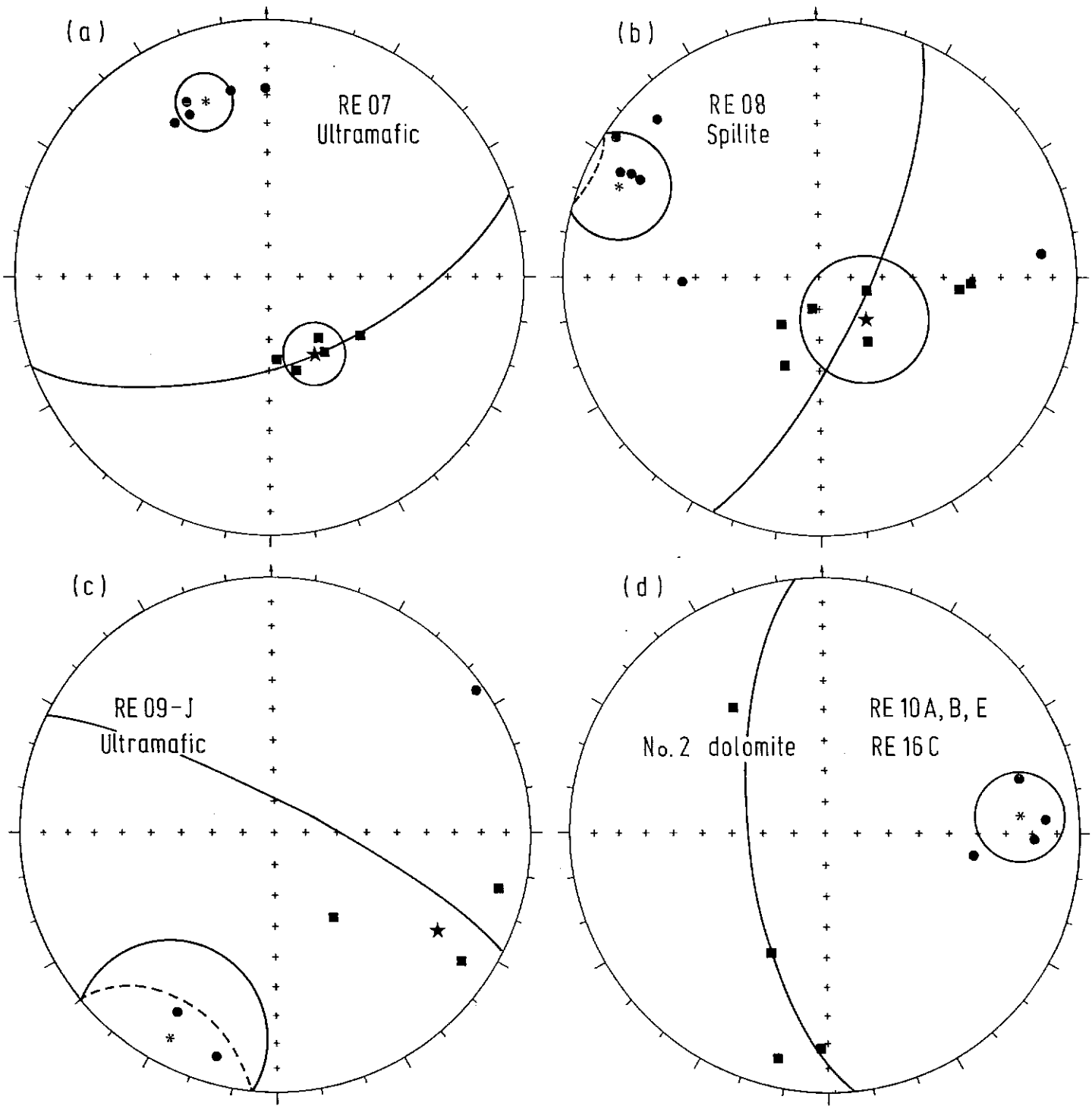
(a)
RE 07
Ultramafic
(b)
RE 08
Spilite
(c)
RE 09-J
Ultramafic
(d)
No. 2 dolomite
RE 10A, B, E
RE 16C

Fig. 18

Fig. 19 Magnetic fabric of (a) sample RE10C, (b) Sample RE10D, (c) specimens from samples RE15A-C, (d) stratabound ore samples. Symbols as in Fig. 17.

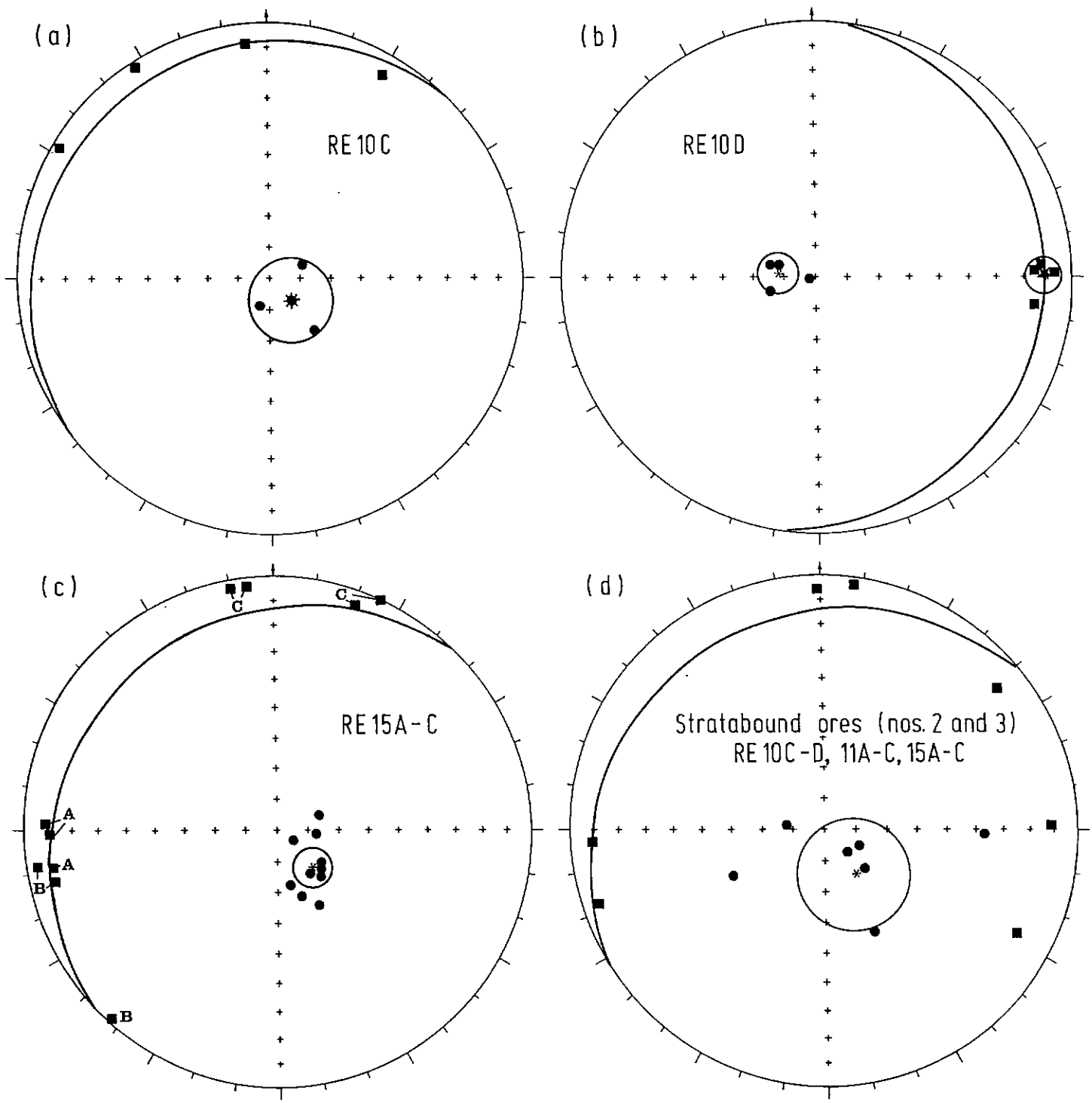
(a)
RE 10C
(b)
RE 10D
(c)
RE 15A-C
A
A
B
B
C
C
(d)
Stratabound ores (nos. 2 and 3)
RE 10C-D, 11A-C, 15A-C

Fig. 19

Fig. 20. Magnetic fabric of (a) Federal ore samples, (b) Melba ore samples, (c) dolerite specimens, (d) Red Rock Member samples. Symbols as in Fig. 17.

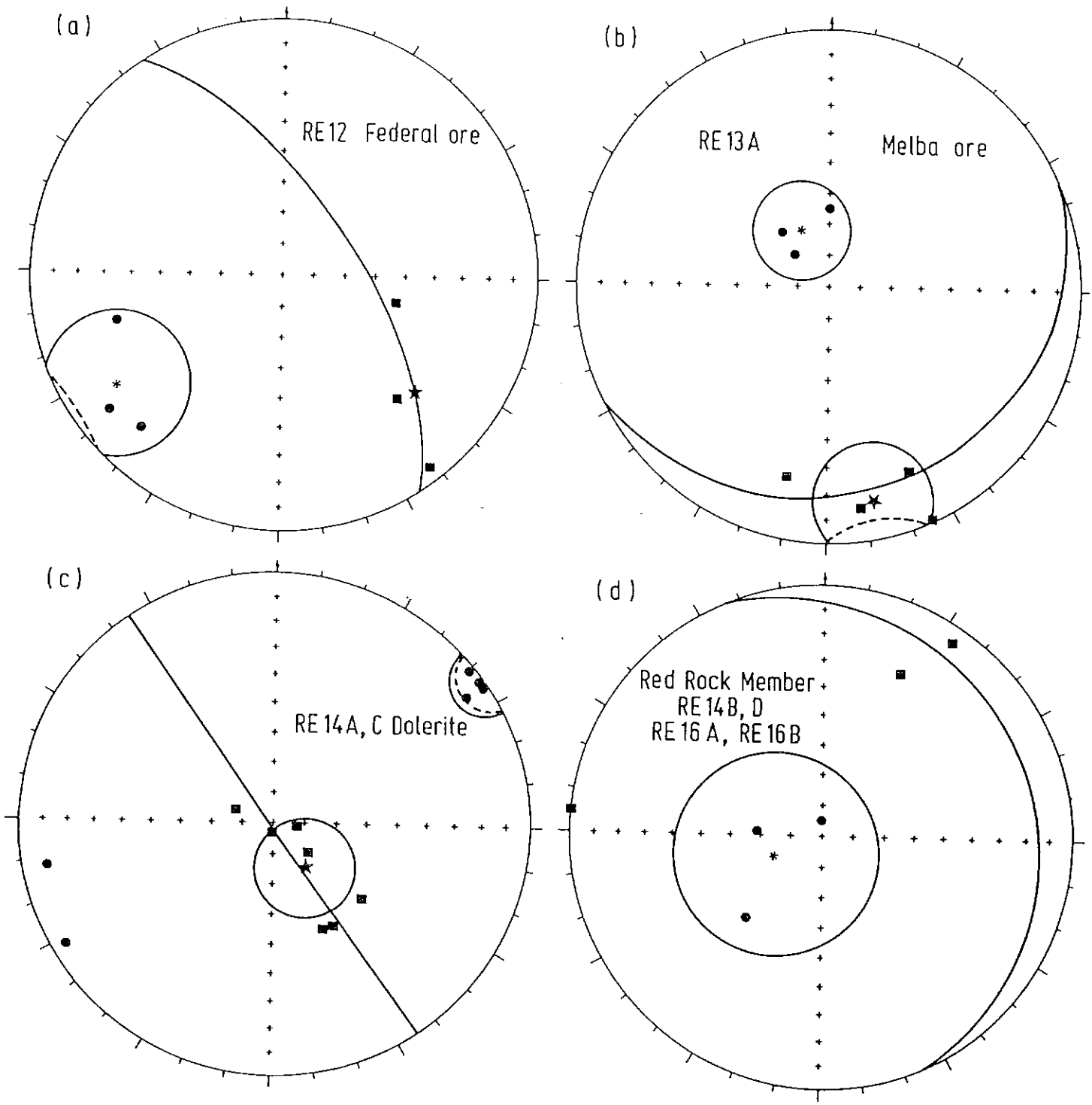
(a)
RE12 Federal ore
(b)
RE13A
Melba ore
(c)
RE14A, C Dolerite
(d)
Red Rock Member
RE14B, D
RE16A, RE16B

Fig. 20